A&A 619, A23 (2018)
https://doi.org/10.1051/0004-6361/201833360

Astronomy & Astrophysics

A MST catalogue of γ-ray source candidates above 10 GeV and at Galactic latitudes higher than 20°★

R. Campana[1], E. Massaro[2,3], and E. Bernieri[4,5]

[1] INAF/OAS-Bologna, via Piero Gobetti 101, 40129 Bologna, Italy
e-mail: campana@iasfbo.inaf.it
[2] INAF/IAPS, via Fosso del Cavaliere 100, 00133 Roma, Italy
[3] In Unam Sapientiam, Piazzale A. Moro 2, 00185 Roma, Italy
[4] INFN-Sezione di Roma Tre, via della Vasca Navale 84, 00146 Roma, Italy
[5] Dipartimento di Matematica e Fisica, Università Roma Tre, Roma, Italy

Received 4 May 2018 / Accepted 1 August 2018

ABSTRACT

We describe a catalogue of γ-ray source candidates selected using the minimum spanning tree (MST) algorithm on the nine year *Fermi*-LAT sky (Pass 8) at energies higher than 10 GeV. The extragalactic sky at absolute Galactic latitudes above 20° has been investigated using rather restrictive selection criteria, resulting in a total sample of 1342 sources. Of these, 249 are new detections that have not been previously associated with γ-ray catalogues. A large portion of these candidates have interesting counterparts, which are most likely blazars. In this paper, we report the main results of the catalogue selection and search of counterparts.

Key words. gamma rays: general – gamma rays: galaxies – methods: data analysis

1. Introduction

The Large Area Telescope (LAT; Ackermann et al. 2012) on board the *Fermi* mission has been continuously observing the sky at energies higher than ∼100 MeV since the beginning of August 2008. This mission has collected a very large number of photons and enriched our knowledge on Galactic and extragalactic high-energy astrophysics. One of the most relevant achievements of this mission is the discovery of thousands of new celestial sources of γ-rays, which have been reported in several catalogues covering different time windows, energy ranges, and source types.

Various methods for detecting point-like sources against the photon and instrumental background are based on the search of local concentrations of γ-rays. Besides the traditional maximum likelihood (ML) algorithm (Mattox et al. 1996), other methods include the use of wavelet transform (Damiani et al. 1997; Ciprini et al. 2007), the density-based clustering algorithm DBSCAN (Tramacere & Vecchio 2013; Armstrong et al. 2015) the Bayesian inferential D^{3}PO algorithm (Selig et al. 2015), and FermiFAST, recently proposed by Asvathaman et al. (2017).

One method, which was initially proposed by Di Gesù & Sacco (1983) for the analysis of data from the COS B satellite (Bignami et al. 1975), is based on an application of the topometric minimum (or minimal) spanning tree (hereafter, MST) algorithm, which has its roots in graph theory. Campana et al. (2008, 2013) developed this method and introduced new estimators for the cluster significance to be applied to γ-ray two-dimensional images in which the points correspond to the arrival directions of photons. The MST method was applied to search source seeds in preparation of the early *Fermi* catalogues (1FGL; Abdo et al. 2010; 2FGL, Nolan et al. 2012; 1FHL, Ackermann et al. 2013b). In a subsequent series of papers (Campana et al. 2015, 2016a,b,c; hereafter Papers I–IV) we analysed the *Fermi*-LAT dataset by means of MST and found several significant γ-ray photon overdensities associated with blazars previously not known as high-energy sources.

In this paper we report a new catalogue of γ-ray clusters, which are robust point-like source candidates that were selected using the MST algorithm in the sky at Galactic latitudes $|b| > 20°$ and at energies higher than 10 GeV. In this work we considered the Pass 8 *Fermi*-LAT photons observed since the beginning of the mission up to August 2017, thus covering a period of nine years. The aim of our search was to enrich the population of weak high-energy sources and to search for their possible counterparts, particularly among confirmed and candidate blazars, which constitute the most numerous class of extragalactic γ-ray sources.

Our sample contains 1342 entries: about 81% of these have a close spatial association with known γ-ray sources reported in public catalogues or surveys, and a further ∼8% can be associated with known and candidate blazars not previously known as γ-ray emitters.

In Sect. 2 the MST method is briefly outlined; in Sect. 3 the data reduction, MST analysis, and selection tools are described. The catalogue content and characteristics are described in the following sections, and in Sect. 9 we discuss our results.

2. Photon cluster detection with the MST algorithm

The MST (Campana et al. 2008, 2013) is a cluster-detection algorithm useful for searching spatial concentrations in a field of points. As stated in the Introduction, we already applied

★ The catalogue is only available at the CDS via anonymous ftp to cdsarc.u-strasbg.fr (130.79.128.5) or via http://cdsarc.u-strasbg.fr/viz-bin/qcat?J/A+A/619/A23

Table 1. Summary of the main parameters in the MST source detection algorithm and their meaning.

Parameter	Meaning
Λ_m	Mean edge length in the MST built on a given field.
$\Lambda_{\rm cut}$	Cut length for the primary selection (e.g. defined as a fraction of Λ_m).
$N_{\rm cut}$	Minimum number of nodes for the primary selection.
N	Number of nodes for a cluster.
g	Clustering parameter, the ratio of Λ_m in the field to the mean edge length in the cluster.
M	Magnitude of the cluster, defined as $M = Ng$.
R_m	Median radius, the distance from the cluster centroid containing 50% of the photons.
$R_{\rm max}$	Maximum radius, the distance from the cluster centroid to its farthest photon.

this method to the γ-ray sky and detailed descriptions of the MST and the selection criteria were presented elsewhere (e.g. in Paper I), therefore, in this work we provide only a brief summary of this method.

Consider a two-dimensional set of n points or nodes: several sets $\{\lambda_i\}$ of weighted edges connecting these nodes can be defined. For a set of points in a Cartesian frame, the edges are the segments joining the nodes and the weights are their Euclidean lengths, while for a region on the celestial sphere the edge weights are the angular distances between pairs of photons. The MST is defined as a (unique) tree, i.e. a graph connecting all the nodes without closed loops, which has a minimum total weight defined as $\min[\Sigma_i \lambda_i]$.

Once the MST is computed by means, for example, of the Prim algorithm (Prim 1957), a set of subtrees corresponding to clusters of photons is extracted by means of a twofold selection, consisting firstly of a separation, removing all the edges having a length $\lambda > \Lambda_{\rm cut}$. The separation value can be defined in units of the mean edge length $\Lambda_m = (\Sigma_i \lambda_i)/n$. This results in a set of disconnected subtrees; then, an elimination removes all the subtrees that have a number of nodes $N \leq N_{\rm cut}$, leaving only the clusters over a fixed threshold in size. The remaining set of subtrees provides a first list of candidate clusters and a secondary selection is applied to extract the most robust candidates as γ-ray sources. A suitable parameter for this selection (Campana et al. 2013) is the clustering parameter g_k defined as the ratio of Λ_m to $\lambda_{m,k}$, the mean length of the kth cluster edges. Another very useful parameter for assessing the significance of the surviving clusters is the cluster magnitude

$$M_k = N_k g_k, \quad (1)$$

where N_k is the number of nodes in the cluster k and g_k its clustering parameter. The probability to obtain a given magnitude value combines that of selecting a cluster with N_k nodes together with its "clumpiness", compared to the mean separation in the field. It was found that $\sqrt{M}$ is a good estimator of statistical significance of MST clusters (Campana et al. 2013). In particular, a lower threshold value of M around 15–20 would reject the large majority of spurious (low significance) clusters.

The cluster centroid coordinates are obtained by means of a weighted mean of the coordinates of the photons (Campana et al. 2013). If the cluster can be associated with a genuine point-like γ-ray source, the radius of the circle centred at the centroid that contains 50% of the photons in the cluster, the median radius R_m, should be smaller than or comparable to the 68% containment radius of instrumental point spread function (PSF; see Ackermann et al. 2013a). Another useful parameter is the maximum radius $R_{\rm max}$, defined as the angular distance between the centroid and the farthest photon, giving information regarding the overall extension of the cluster. Table 1 reports a summary of the main parameters in the MST source detection algorithm.

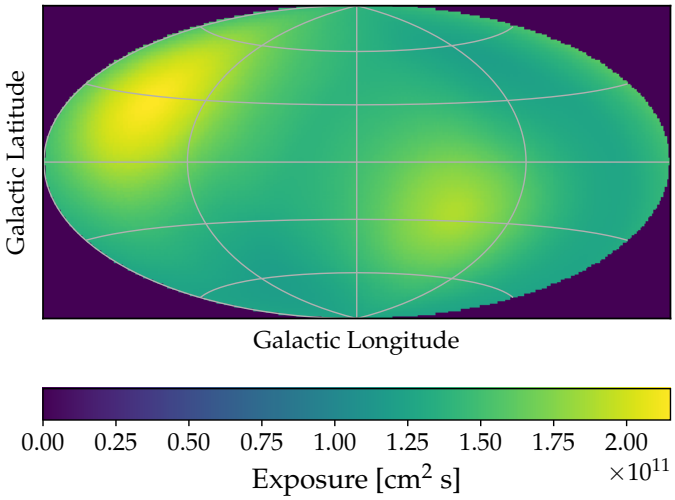

Fig. 1. Sky map of the *Fermi*-LAT exposure at 10 GeV in the first 9 years of observation in scanning mode.

3. The MST catalogue

3.1. The Fermi-LAT dataset

The full *Fermi*-LAT dataset collected above 10 GeV in the nine years from 2008 August 4 to 2017 August 4, and processed with the Pass 8 reconstruction algorithm and responses, was downloaded from the FSSC archive[1]. The standard cuts on data quality and zenith angle (SOURCE class events, front and back converting, up to a maximum zenith angle of 90°) were applied.

The scanning mode of *Fermi*-LAT resulted in a non-uniform exposure distribution over the sky with a maximum value near the north celestial pole and minimum exposure on the celestial equator, as apparent in the map reported in Fig. 1.

The detection of photon clusters, performed by means of MST, depends upon the mean spatial density of background events, which largely increases moving from the Galactic poles to the equator. For this reason we removed from the data the region with $|b| < 19°$, where the clusters found (in particular those with a small number of photons) are not sufficiently stable, i.e. their number of photons changes drastically even for small variations of the $\Lambda_{\rm cut}$ parameter. The final dataset contains 291 979 photons, of which 152 906 and 139 073 are in the north and south Galactic regions, respectively. This difference is mainly due to the non-uniform spatial distribution of the exposure.

3.2. Primary selection

To take into account the differences in the photon density, we divided the full non-Galactic sky into three strips 17° wide in Galactic latitude for each hemisphere, allowing for a 2° overlap between the adjacent regions. The boundaries of these regions are illustrated in the sky map in Fig. 2. The strip nearest to the

[1] http://fermi.gsfc.nasa.gov/ssc/data/access/

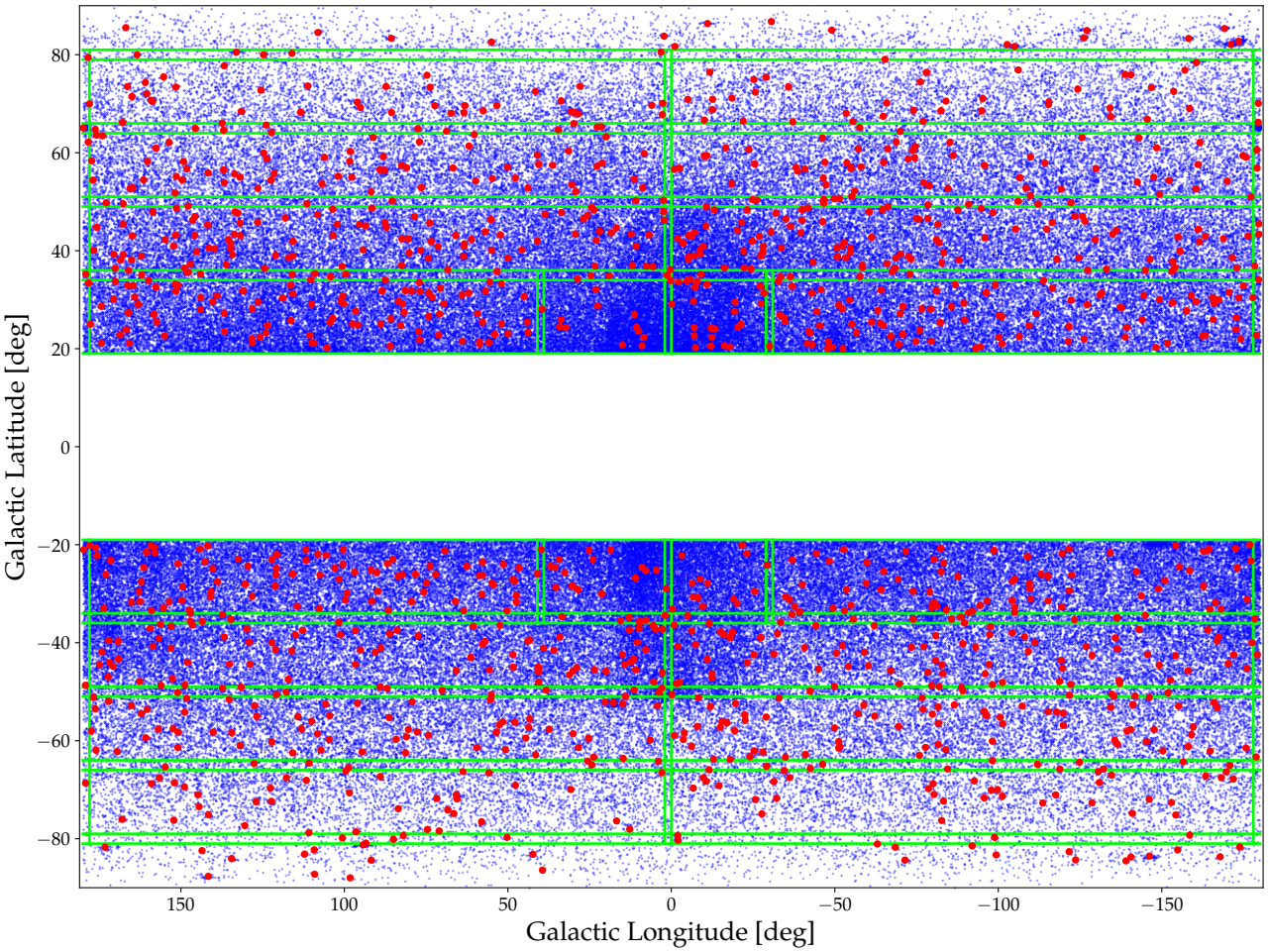

Fig. 2. Sky map of the photons in the 10–300 GeV energy range considered in our analysis. Green lines indicate the boundaries of the regions used for the MST cluster search. Red dots are the clusters given in the final 9Y-MST catalogue.

Galaxy was subdivided in four longitude sectors, while the other two strips were split in two sectors. The north and south Galactic polar regions ($|b| > 79°$) were analysed separately.

For each field the MST was computed on the unbinned photon maps applying a primary selection using $\Lambda_{\rm cut} = 0.7\,\Lambda_m$ and $N_{\rm cut} = 3$. These values have been shown (Campana et al. 2015, 2016a) to be rather optimal for further selections. The resulting cluster samples were merged and a first preliminary list of 6503 clusters was obtained. The selected regions, their solid angles, photon numbers, and the used absolute $\Lambda_{\rm cut}$ are summarized in Table 2; we also report the number of clusters $N_{\rm ps}$ found in each region with only the primary selection. We note that the separation length, when measured in arcmin, remains uniform in many regions with the exception of the southern highest latitude belt and polar region, where it is longer than 10′ since these fields are more sparse than the northern counterpart, and therefore also larger than the PSF radius. As a consequence of this fact, in these three regions the number of clusters is much higher than in the corresponding northern regions despite the lower photon numbers.

3.3. Secondary selections

We applied firstly a uniform secondary selection over the entire cluster dataset. We assumed a threshold value of $M > 15$, while for the four-photon clusters only ($N = 4$) a looser threshold of $M > 12$ was applied to take into account all those having $g > 3$. Moreover, multiple coincident clusters in the overlapping regions were eliminated taking only those with the highest M. We thus obtained a list of 2153 candidate sources.

We then applied a further "superselection" using different criteria for different sky regions. This has been proved to be an efficient strategy to take into account the backgrond non-uniformities, especially in peri-Galactic regions and in the so-called *Fermi* Bubbles (Su et al. 2010), and to increase the chance to select clusters corresponding to genuine candidate γ-ray sources. We note that with the superselection we further restrict the analysis to Galactic latitudes $|b| > 20°$.

We defined the following four regions and characterized each region by a specific threshold on M and g:

1. High latitudes and poles, $|b| > 50°$: $M > 18$ or $g > 3.5$;
2. Middle latitudes, $30° < |b| < 50°$: $M > 20$ or $g > 4.0$;
3. External peri-Galactic belt, $20° < |b| < 30°$ with $0° < L < 330°$: $M > 22$ or $g > 4.2$;
4. Central peri-Galactic belt, $20° < |b| < 30°$ with $-30° < L < 30°$: $M > 24$ or $g > 5.0$.

We note that the "or" above is to be intended in Boolean sense, i.e. for the Galactic poles we select the clusters that have either $M > 18$ or $g > 3.5$.

The choice of these superselection parameters was based on the experience from previous analyses, aiming at selecting a population having a large majority of significant structures and

Table 2. Sky regions used in the MST search for photon clusters.

Region	Solid angle	Photon number		Λ_{cut}		N_{ps}		N_{ss}	
	sr	N	S	N	S	N	S	N	S
$\|b\| > 79°$	0.1154	4639	3162	7.4	13.3	58	127	20	28
$64° < \|b\| < 81°$ A	0.2824	10521	6428	6.8	10.1	102	138	45	42
$64° < \|b\| < 81°$ B	0.2955	9498	6014	7.5	10.5	105	154	42	44
$49° < \|b\| < 66°$ A	0.5045	17267	14297	7.4	8.7	197	278	71	75
$49° < \|b\| < 66°$ B	0.5101	16361	12570	7.9	9.4	228	266	65	81
$34° < \|b\| < 51°$ A	0.6923	24822	24121	7.6	8.0	425	512	110	93
$34° < \|b\| < 51°$ B	0.6999	23126	21469	8.2	8.4	564	435	107	86
$19° < \|b\| < 36°$ C	0.1876	11769	10209	6.1	6.5	298	252	17	20
$19° < \|b\| < 36°$ D	0.6544	25942	24282	7.4	7.8	466	510	94	89
$19° < \|b\| < 36°$ E	0.7002	22555	25512	8.4	7.8	494	539	96	78
$19° < \|b\| < 36°$ F	0.1510	9368	7060	5.9	6.8	208	147	24	15

Notes. There is an overlap on each side of the regions. The total number of photons and the resulting separation lengths for the north and south Galactic regions are given; the well evident N-S asymmetry is mainly because of the different exposures. In the last two columns the number of clusters found in each region are reported with the primary selection and after the application of the secondary and superselection, as described in the text. The Galactic longitude intervals are A: $0° < l < 182°$; B: $178° < l < 362°$; C: $0° < l < 41°$; D: $39° < l < 182°$; E: $178° < l < 331°$; and F: $329° < l < 362°$.

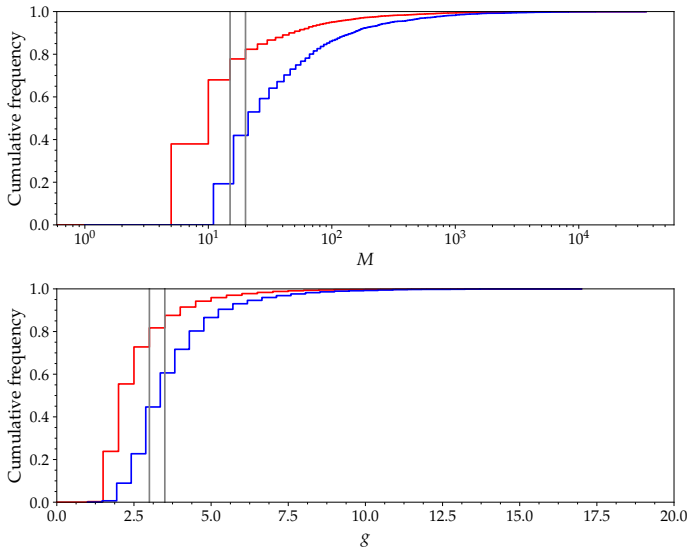

Fig. 3. *Upper panel*: cumulative distributions of the magnitude M of the clusters after the primary (red) and secondary (blue) selections. Vertical bars correspond to the cuts $M > 15.0$ and $M > 20.0$. *Lower panel*: cumulative distributions of the clustering parameter g of the same cluster sets. Vertical bar corresponds to the selection thresholds $g > 3.0$ and $g > 3.5$.

is further justified in the following Sect. 3.4. The cumulative distributions of the cluster parameters M and g are shown in the two panels of Fig. 3, after the primary and secondary selections. In the figure some representative cut levels are indicated, showing that the percentage of surviving clusters after both selections.

The validity of our selection criteria is further confirmed by the percentage of clusters with associations to known sources or other interesting objects, higher than 95%, as discussed in the following sections.

After applying these criteria the number of candidate sources is reduced to 1342. This number, about 20% of the original primary selection clusters, is therefore comparable (i.e. about the same order of magnitude) to the amount of sources already detected in the same sky region, for example in the 3FHL or 3FGL catalogues. The distribution of these clusters into the regions used in our analysis is also given in Table 2 as N_{ss}, not including double and multiple detections in the overlapping areas. It is interesting to note how the large excesses of clusters after the primary selection in the regions with a low photon number is now largely reduced. The superselection is therefore able to clean up the majority of low significance strucures, up to about 90% in some regions. Of course, we cannot exclude that a fraction of clusters associated with genuine high-energy sources is also eliminated, but such a choice is a necessary trade off for obtaining a good sample of significant clusters.

These clusters are all included in the nine year MST (9Y-MST) catalogue FITS file available as additional electronic material[2]. The FITS contains cluster information (coordinates, N, g, M, R_m, and R_{max}) and the associated counterparts discussed in the following sections. The sky map of the clusters is shown in Fig. 2. The distributions of the N, g, and M parameters for all the 9Y-MST sources are shown in Fig. 4, while those of R_m and R_{max} are given in Fig. 5.

We note that there are a few very rich clusters ($N > 100$) and, in particular, only two have more than 1000 photons and are associated with two well-studied BL Lac objects: PG 1553+113 (5BZB J1555+1111) with 1010 photons, and Mrk 421 (5BZB J1104+3812) with 1997 photons. The R_m and R_{max} distributions are remarkably different, since the latter is peaked around 10′ and extends up to 55′, while more than 96% of clusters have $R_m < 8'$.

The scatter plots of the radii (R_m and R_{max}) versus the cluster photon number are shown in Fig. 6. Their difference is clear: in particular, for the richest clusters R_m is very close to 4.5, while the maximum radius is an order of magnitude larger. This finding indicates that in the surroundings of large clusters there is a tendency to find angular distances that are shorter than Λ_m in the entire region with the aggregation of extended haloes. An interesting case is that of clusters with a rather low number of photons but a large R_m. These clusters could be either

[2] The catalogue is also available at the URL: http://www.iasfbo.inaf.it/~campana/9Y-MST_catalogue_latest.fits

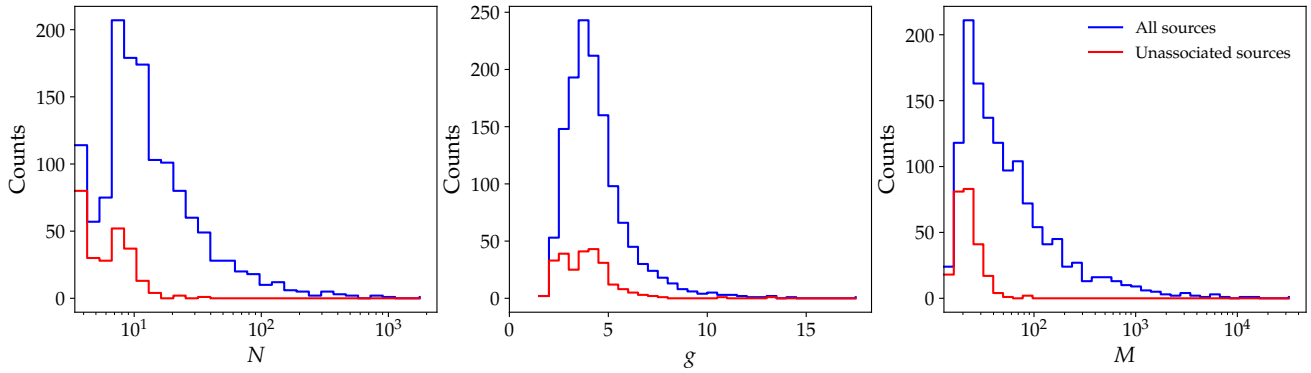

Fig. 4. Distribution of the N, g, and M parameters for all the 9Y-MST sources (blue histograms) and for the unassociated sources only (red histograms, see main text for details).

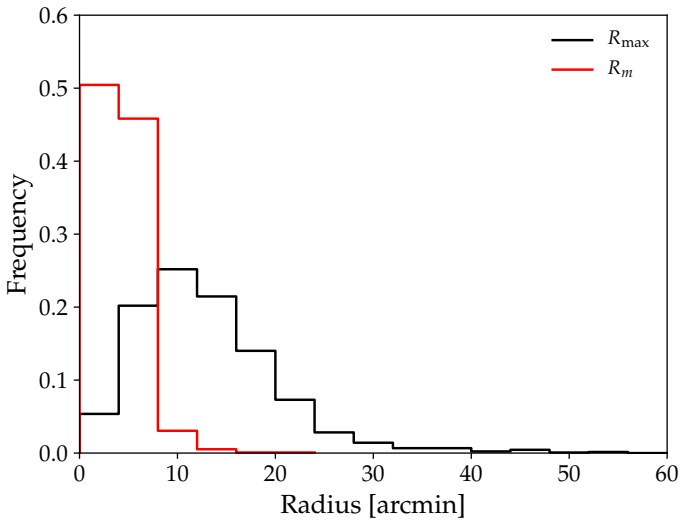

Fig. 5. Distributions of R_{max} (black histogram) and R_m (red histogram) for all the 9Y-MST sources. Nearly all clusters have R_m values smaller than 8′, while the other distribution is peaked around 10′.

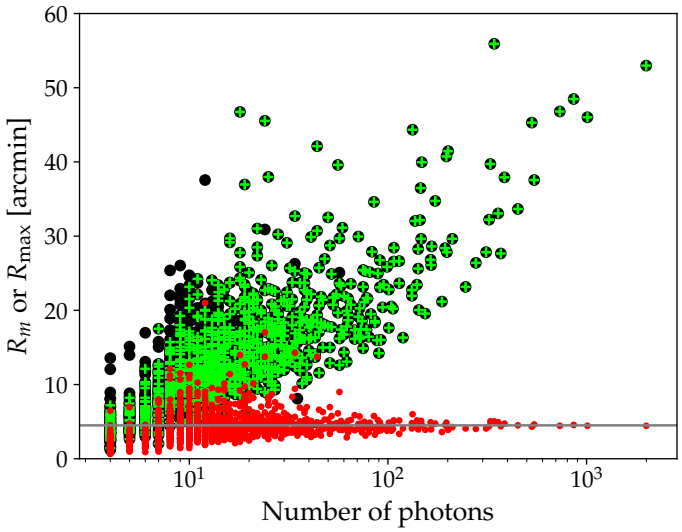

Fig. 6. Scatter plots of the maximum radius R_{max} (black points) and of the mean radius R_M (red points) vs. the number of photons in the clusters for all the 9Y-MST sources. We note that for high photon number the mean radius is very close the constant value of 4′.5 (horizontal line). Green crosses overlaid on the black points indicate the 3FGL counterparts to the 9Y-MST clusters.

extended structures or those with a denser subcluster associated with nearby background photons. In general these clusters are also characterized by a low clustering factor, and their properties are discussed in Sect. 6.2. Another item to take into account is the possibility to find small spurious clusters in the close surroundings of a very rich cluster: for this to occur, it is enough to cut only one edge connecting the two structures. The usual terminology is to call these "satellite" clusters of the main cluster; see Campana et al. (2013). This matter is further discussed in Sect. 8.

3.4. Occurrence of spurious clusters

The above discussed superselection rules were chosen and applied to reduce the possibility to include clusters originated by local fluctuations of the background in the final sample, i.e. spurious clusters not corresponding to a real source. Evaluating the expected fraction of spurious structures in the catalogue is a complex task, but an estimate is useful to understand the quality of the selection methods. Campana et al. (2013), on the basis of simulations with random fields, found that selections with thresholds on M ranging from 15 to 20 produce a low fraction ($\lesssim$10%) of these spurious clusters. However, simply using a high M selection threshold does not give particularly interesting results, since the most likely outcome is a sample containing bright sources that can be found with any other method. Our main goal is to select clusters that can be associated with new sources: this implies that they can also have a low photon number. For these reasons we also applied a selection on g. Moreover, we have to consider the possibility to select structures with M values above the threshold but with low clustering as expected from extended or "confused" features.

To evaluate the expected fraction of spurious clusters we performed numerical simulations on a photon background similar to that observed. A simulated nine year >10 GeV *Fermi*-LAT sky was generated using the `gtobssim` tool[3], including only the Galactic and isotropic diffuse backgrounds (`gll_iem_v06` and `iso_P8R2_SOURCE_V6_v06`) and assuming the same spacecraft attitude as the actual dataset. The MST algorithm was applied using the same procedure and primary selection parameters as for the real data: in particular, the absolute value of Λ_{cut}, i.e.

[3] https://fermi.gsfc.nasa.gov/ssc/data/analysis/scitools/help/gtobssim.txt

measured in degrees, was fixed to the adopted value in the selection on the true field. Afterwards, the superselection criteria were applied to the simulated data as well. The resulting percentage of spurious clusters surviving to this procedure was ∼4%. This implies that an estimate of the possible spurious cluster between the 1342 entries in the catalogue gives a number of about 55 clusters, most of which have 4 or 5 photons. However, slightly higher numbers of spurious clusters cannot be excluded, since the presence of many rich clusters in the true sky affects the MST construction in a way that it is difficult to reproduce in any simulation.

Other spurious clusters can be present if there are significant photon density gradients, as observed in the regions near the Galactic belt, where it is possible to select low g clusters close to the low $|b|$ boundaries where the photon density increases. Not all these clusters may be spurious. Some could be associated with real sources, considering that the number of Galactic γ-ray emitters can also increase at low latitudes. In these cases, an analysis of small regions (typically having a size of $10^\circ \times 10^\circ$) with decreasing $\Lambda_{\rm cut}$ values can help to verify whether these structures remain stable or they dissolve into the background. In the latter occurrence, this is a strong indication that the cluster could be spurious. In the catalogue, a flag is reported in these ∼20 cases.

4. Correspondence between 9Y-MST and *Fermi* catalogues

We searched for the correspondences between our 9Y-MST clusters with the two most recent main catalogues published by the *Fermi* collaboration: the 3FGL catalogue (Acero et al. 2015), including 3034 γ-ray sources detected in the energy range $0.1 < E < 300$ GeV; and the 3FHL catalogue (Ajello et al. 2017), including 1556 sources at energies higher than 10 GeV. The former catalogue was based on the first four years of LAT data, while the latter considered photons detected in a time interval of seven years. The sources in these two catalogues are distributed over all the sky and there are 1715 and 986 for the 3FGL and 3FHL, respectively, in the same field considered for the MST catalogue with $|b| > 20^\circ$.

4.1. 3FHL catalogue

We searched first the associations of 9Y-MST clusters with the 3FHL catalogue because of their similar energy ranges, within a maximum separation of 20′, and obtained 923 correspondences. The distribution of the separations is shown by the red histogram in Fig. 7. About all the sources (916, 99.2%) are found within a maximum distance δ of 6′. We can conclude that this value can be adopted in other searches when at least one of the source positions is known with a much higher precision, as in the case of optical or radio catalogues. In the search for associations between MST clusters and 3FHL sources the choice of a matching radius of 6′ (0.°1) can be also based on the distribution of the semimajor axis of positional error ellipse at 95% confidence of the 3FHL sources ("Conf_95_SemiMajor" parameter in the 3FHL catalogue), which is smaller than this value for almost all (>99.3%) sources.

For farther distances, at $\delta = 6\farcm5$ there is only one cluster associated with a 3FHL source: 9Y-MST J0529−6904, which has 34 photons and $R_{\rm max} = 26\farcm3$. This is an indication that it is clearly extended because it is also located within the Large Magellanic Cloud. No sources are found with $6\farcm5 < \delta < 10'$.

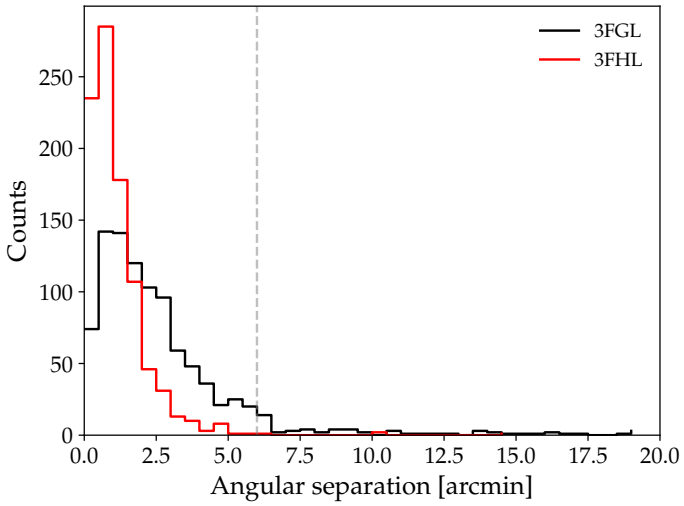

Fig. 7. Histograms of the angular distances δ between the clusters in the 9Y-MST catalogue and the sources in the 3FHL (red) and 3FGL (black) catalogues. The dashed vertical line indicates the matching distance of 6′ assumed for the 3FHL associations.

At larger angular separations, $10' < \delta < 20'$, we have six possible matches. Five are multiple associations (i.e. there is another 3FHL source within 20′ from the 9Y-MST cluster, or vice versa), and only one is a single association. The latter is the cluster located at RA = 269.°959; Dec = 70.°612 at an angular distance of 14.′6 from 3FHL J1757.7031 (corresponding to 3FGL J1756.9+7032), which has the BL Lac counterpart 5BZB J1757+7033; this angular distance appeared too large for a correct matching and we verified that there is a cluster very close to the 3FHL source position with seven photons and $M = 21.71$, just below the superselection threshold for this region. We, therefore, considered the cluster as not associated with the 3FHL source and included it in the catalogue; we stress that this choice is strengthened by the fact that it is at 1.′1 to the other BL Lac object 5BZB J1759+7037. The angular separation distribution thus indicates that the correct matching distance for the search of counterparts is within 6′ and that the few sources found at higher separations are either random associations or peculiar occurrences.

It is clear that such a high percentage of associations cannot be due to chance correspondences between the two catalogues. However, it cannot be excluded that some associations might actually be spurious. We therefore evaluated how many correspondences are expected from a cross matching of two catalogues with similar large scale distributions. We thus constructed a set of fake catalogues with the same number of 9Y-MST clusters but coordinates shifted in RA and Dec by variable amounts ranging from 0.°5 to 3.°5. The cross-matching analysis with the true 3FHL catalogue within 6′ gave a number of correspondences ranging from 0 to 4, with a mean value equal to 1.5 and a standard deviation of 1.35. Thus, it is reasonable to consider as genuine all 916 associations (92.9% of the 3FHL catalogue sources). For a further discussion on the matching radius, see also Campana et al. (2015).

We then searched for the remaining 70 not associated 3FHL sources in the initial list of 2153 pre-superselection clusters, and 60 corresponding associations were found. These clusters were excluded from the 9Y-MST catalogue because they do not fulfil the requested severe selection criteria. In particular, although nine of them had $M > 22.0$ or $g > 4.2$ they

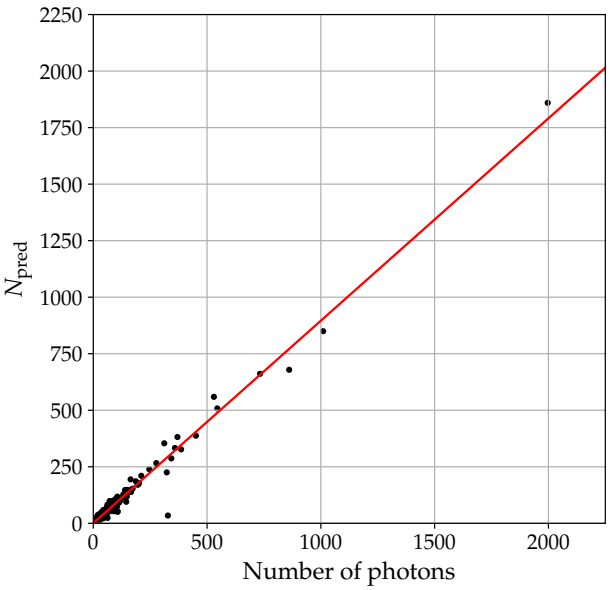

Fig. 8. Number of photons N for the 9Y-MST clusters with a 3FHL counterpart vs. the number of ML predicted photons $N_{\rm pred}$. The red line is the linear best fit.

were however rejected being located in the region near the Galactic Bulge.

Therefore, there are only 10 3FHL sources not associated with MST clusters: all of these sources are reported in the 3FHL with usually a rather low significance. We can then conclude that ~99% of the 3FHL sources were found by our MST method and a further ~6% were rejected by the superselection criteria.

It is interesting to compare, for the matching MST-3FHL clusters, their number of photons N with the number of predicted photons $N_{\rm pred}$ from the ML analysis, reported in the 3FHL catalogue. Figure 8 shows this comparison: an excellent linear agreement with the two quantities is found with a slope ~0.9 and an intercept compatible with 0 at the 2σ level. The only significant outlier is 3FHL J2232.7+1143, for which a cluster with 328 photons ($M \sim 3120$) is found but the 3FHL catalogue reports $N_{\rm pred} = 34.17$. This source (also known as CTA 102) had a significant outburst in late 2016, thus outside the 3FHL data range.

4.2. 3FGL catalogue

The search for associations between MST clusters and the 1715 3FGL sources in the same sky region resulted in 943 matchings within a maximum angular separation of 20′ (55.2%, Fig. 7). The fact that many sources of this catalogue are not associated with clusters is likely a consequence of the different energy ranges considered: the majority of the photons for the 3FGL sources have energies below 10 GeV down to 100 MeV. Moreover, the use of lower energy bands (characterized by a broader PSF) loosens the positional accuracy of the 3FGL sources, allowing for higher δ values. This is apparent from the δ distribution (black histogram in Fig. 7), which is much broader with respect to the 3FHL sources.

In this case, we can consider $\delta = 15'$ as the threshold for a genuine association with the 3FGL catalogue. We note that about 96% of the sources in the 3FGL catalogue have a positional error ellipse semimajor axis smaller than this value.

There are 2 MST sources that could be associated within 15′ from the 3FGL J0849.3+0458 source, 9Y-MST J0849+0456 at $\delta = 6\farcm2$ and 9Y-MST J0848+0507 at $\delta = 13\farcm2$. At a closer look to the photon distributions, it is clear that these are two distinct associations; the 3FGL source is associated with the closer MST cluster, while the farthest cluster has a very good association with a 3FHL source (3FHL J0848.7+0508).

There are only 8 sources with $15' < \delta < 18'$. It is possible that some of this group are spurious associations, and therefore they are examined in the next subsection. Interestingly, 783 sources (i.e. about 83% of the entire sample) are found within $\delta < 4'$, and 885 (~94%) within $\delta < 6'$ confirming the accuracy of these positional estimates.

Thus, we consider as genuine 935 associations with the 3FGL catalogue (within 18′, 54.5% of the sample). Finally, we note that only 792 of the 935 associated 3FGL sources are also in the 3FHL catalogue within a distance of 6′. Thus, with the MST method, above 10 GeV, 143 3FGL sources not previously found in the 3FHL are detected. The total number of clusters in the 9Y-MST associated with either 3FHL or 3FGL is thus equal to 1060.

4.3. Possible association with 3FGL sources at large angular distances

As mentioned above, eight 9Y-MST clusters have angular distances from possible 3FGL counterparts greater than 15′ but smaller than 18′. An effective way to investigate the robustness of these associations is to perform a MST analysis on smaller fields around the possible associations, usually a few degrees wide. For a likely genuine association, the centroid of the MST cluster shall become closer to the counterpart and the cluster shall remain usually stable for different choices of $\Lambda_{\rm cut}$.

While one of these clusters (9Y-MST J0233+0656) has a much closer 3FHL counterpart, i.e. the more distant 3FGL association is very likely spurious, in three cases (9Y-MST J0009−1418, 9Y-MST J1202+3857, and 9Y-MST J1553−0305) the cluster remains at a wide or even increasing separation from the 3FGL counterpart for various choices of the surrounding field dimension and/or $\Lambda_{\rm cut}$. We therefore discard these possible associations as spurious.

The MST cluster separation from the 3FGL sources decreases (down to a few arcmin) only in two cases: 9Y-MST J1336−4043 associated with 3FGL J1335.2−4056 and 9Y-MST J2127−3940 associated with 3FGL J2126.5−3926. Thus we retain these associations.

Finally, there are two 3FGL sources associated with 9Y-MST cluster pairs: 3FGL J1150.5+4155 and 3FGL J0843.4+6713. At a separation of $1\farcm48$ from 3FGL J1150.5+4155, which has a well established counterpart in the bright BL Lac object 5BZB J1150+4154, there is the very rich cluster 9Y-MST J1150+4154 with 86 photons and $R_{\rm max} = 18\farcm5$ while the much smaller 9Y-MST J1150+4209 with only 4 photons and a low $M = 17.27$ is located at $15\farcm28$. There are no interesting possible counterparts for the latter cluster, which can be reasonably considered as a satellite of the former. The other case is that of 3FGL J0843.4+6713, without any reported counterpart, which has two nearby clusters: 9Y-MST J0843+6713 ($N = 10$; $M = 27.87$) at the very small angular distance between the centroids of 8″ and 9Y-MST J0842+6656 ($N = 9$; $M = 32.03$, with $\delta = 17\farcm24$) and a close 3FHL association. Such a large difference in angular separations and the low probability ratio that the associated cluster is more distant ($\approx 6 \times 10^{-5}$, estimated from the area ratio of the circles spanned by the two distances), indicates that the former is more likely associated with the 3FGL source.

4.4. 2FGL and 1FGL catalogues

A further search for associations within 18′ with the 2FGL catalogue (Nolan et al. 2012, two years of observations, 1024 sources in the sky region under investigation) and 1FGL catalogue (1FGL, 11 months of observations, 806 sources in the same sky region) revealed two further associations: 9Y-MST J0723+5840 associated with 1FGL J0722.3+5837 and 9Y-MST J0952+3931 associated with 1FGL J0952.2+392. The total number of clusters in the 9Y-MST associated with either 3FHL or 3FGL/2FGL/1FGL is thus equal to 1064, implying that 79.3% of the 9Y-MST sources have a counterpart in one of the *Fermi*-LAT catalogues.

5. Correspondence between 9Y-MST and other known γ-ray sources

As mentioned in the Introduction, in a series of four papers we applied MST for searching in the LAT sky candidate sources likely associated with blazars at energies higher than 10 GeV. In Paper I we searched in the 6.3 year LAT sky (Pass 7) for clusters that have possible counterparts among the BL Lac objects reported in the fifth edition of the Roma-BZCAT (Massaro et al. 2014, 2015) and found 19 clusters with $5 \leq N \leq 12$ and $15.2 \leq M \leq 36.47$. These sources were verified by means of the standard unbinned likelihood analysis that found 15 sources with $TS \geq 15$, with 7 sources having $TS \geq 25$.

In Papers II, III, and IV a similar analysis was performed on the seven year LAT sky (Pass 8) to search clusters that have an association with the 1WHSP sample (Arsioli et al. 2015), with blazars of different type in the Roma-BZCAT, and with new blazar candidates with mid-IR selection, such as WIBRaLS (D'Abrusco et al. 2014), respectively. These papers collectively reported 71 new clusters with $M > 20$, of which only 3 resulted with likelihood test statistics $TS < 16$, and with 58 having $TS > 25$. Furthermore, 67 of these 71 clusters were confirmed in the subsequent 3FHL catalogue.

In the 9Y-MST catalogue there are 73 clusters within an angular distance of 6′ out of these 90 previously MST-found blazars (Papers I–IV); 3 more clusters are at distances of ∼6.′5, but their $R_{\rm max}$ is higher than 12′ and one also has a R_m as large as 8.′5: therefore, their associations cannot be excluded a priori. Of the remaining 14 non-associated clusters, 7 were reported in Paper I, 3 in Paper III, and 4 in Paper IV.

We verified whether some of these clusters were present in the lists produced with the primary selection and found 12 with M and g values lower than the strict thresholds considered for the superselection, although 8 of these had $M > 15$. Only two clusters, both in Paper I with low TS values (MST 0803+2440 and MST 1311+3951) were not confirmed by the present analysis. It is interesting that MST 1311+3951 is reported in the 3FHL (as 3FHL J1311.7+3954), together with another of these 14 MST blazars (MST 1449+2746 in Paper III, corresponding to 3FHL J1449.5+2745). Therefore, 1073 of the 1342 9Y-MST sources were previously reported in either one of the *Fermi*-LAT catalogues or in Papers I–IV.

Recently, Arsioli & Chang (2017) reported the results of a search for γ-ray emission from blazars and candidates listed in the 2WSHP sample (Chang et al. 2017) and detected a signal in the 0.3–500 GeV band from 150 objects (1BIGB sample) not reported in the 1FGL, 2FGL, and 3FGL catalogues. Twenty-eight of the 1BIGB sources were in the previous lists found by MST analysis (Papers I–IV). Of the 150 1BIGB sources, 51 are also associated with 9Y-MST clusters within a distance of 6′. Of these, 26 out of 28 correspond to Paper I–IV sources, while the other two are below the selection threshold. After the subtraction of these sources we obtained a sample of 252 9Y-MST unassociated clusters.

Other three γ-ray sources were found to be associated with 9Y-MST clusters. One is the famous GRB 130427A (Maselli et al. 2014) clearly detected by *Fermi*-LAT (Ackermann et al. 2014) and corresponding to a cluster of 16 photons ($M = 59.27$) located at 2.′35 from the GRB position. The cluster 9Y-MST 2250−1255 is clearly associated with the flat spectrum radio source PKS 2247−131, without any known optical counterpart. This source had a γ-ray flare in 2016 detected by *Fermi*-LAT (Buson 2016) and the corresponding rich cluster has 25 photons ($M = 94.27$). The third cluster is 9Y-MST J1544−0649 with 22 photons and $M = 96.6$ corresponding to the transient source *Fermi* J1544−0649, which brightened for two consecutive weeks beginning on 2017 May 15 (Ciprini et al. 2017) and was later observed in other bands (Chornock & Margutti 2017; Kawase et al. 2017): this cluster was associated with the galaxy 2MASX J15441967−0649156, which exhibits some blazar properties.

Thus the final list of newly discovered clusters includes 249 objects and it is reported in Table A.1. Two of these sources are located in the LMC, which is a complex and interesting region. A discussion on the counterparts within this region is deferred to another paper (Campana et al. 2018).

The *Fermi*-LAT collaboration has published on-line a preliminary list of γ-ray sources detected in eight years of observation[4]. This FL8Y list will be superseded in the near future by a new official catalogue. This catalogue contains 5524 entries of which 2931 are at Galactic latitudes $|b| > 20°$. We verified how many 9Y-MST clusters have a positional correspondence with sources in this list and found 1177 matches within an angular distance of 8′, including all the correspondences with the 3FGL catalogue. Moreover, in this residual sample we found four 3FHL, one 1BIGB source, and the above reported GRB, reducing thus the number of unassociated clusters to 159. Thus, the percentage of clusters with a confirmed γ-ray counterpart can increase up to about 88%.

6. Particular cluster subsamples

In the full 9Y-MST catalogue there are 449 clusters characterized either by a low number of photons or by a low clustering factor; consequently these sources have values of M that are not high enough to exclude that a fraction of these clusters could not be associated with γ-ray sources, but instead correspond to spurious structures. In Sect. 3.4 we estimated that a percentage of 4% or slightly higher of the total number of catalogue sources is indeed expected to be not genuine. We also note that these subsamples contain about all unassociated clusters. In the following subsections we discuss the properties of these subsamples to achieve some specific indication of whether they are or not originated by random localized fluctuations of the photon density.

6.1. Low N clusters

There are 246 clusters that have less than 7 photons, of which 114 have 4 photons, 57 have 5 photons, and 75 have 6 photons. A large percentage of these clusters are associated with known

[4] https://fermi.gsfc.nasa.gov/ssc/data/access/lat/fl8y/

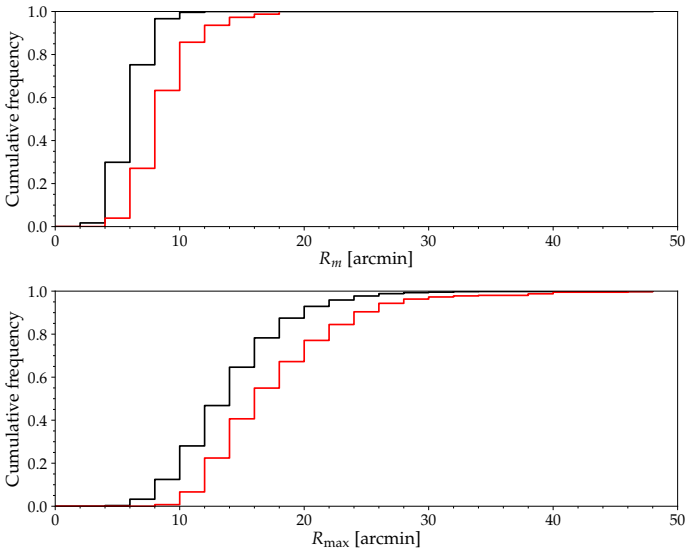

Fig. 9. *Upper panel*: cumulative distributions of R_m for the cluster samples with a photon number in the interval [7, 25] and $g > 3$ (black line) and $g < 3$ (red line). *Lower panel*: cumulative distributions of R_{max} for the same two samples.

γ-ray sources and for several others we found interesting possible counterparts to be confirmed by further investigations. Thus 46 clusters with 6 photons are associated with known γ-ray sources and 15 have candidate counterparts, 26 and 17 are those for the clusters with 5 photons and 33 and 30 are found among the 4 photon clusters. There are 82 low N clusters for which we did not find any association or any candidate counterpart, that is one-third of the entire subsample.

6.2. Low g clusters

There are 203 clusters in the 9Y-MST catalogue with a value of the clustering degree $g < 3.0$ and a minimum number of 7 photons; two are in the Large Magellanic Cloud and are not included in the following analysis, reducing their effective number to 201. In principle, one can expect that this subsample might include a fraction of spurious clusters, not directly related to point-like sources but either to extended region of relatively high photon density, blended pairs of close sources, or single sources near some random concentrations of photons. As discussed in Sect. 3, the disentangling of these situations is not a simple task and a further MST analysis with a shorter Λ_{cut} in a rather small region surrounding the cluster under examination can provide useful information.

The values of R_m and R_{max} of the low g clusters are systematically higher than those of other clusters with a similar photon number but $g > 3$. This is apparent from the cumulative distributions reported in Fig. 9. We note, however, that more than 60% of low g clusters have $R_m < 8'$, which is a value compatible with a point-like source; the large extension of clusters can be understood by the aggregation of a few photons of the local background due to the relatively long local separation length. The number of low g clusters in the residual sample of unassociated entries, after the selection for correspondences with known catalogues and lists (see the previous sections), is equal to 49, about 3.7% of the entire 9Y-MST catalogue and 24% of the subsample. For 14 of these clusters, particularly those with a low R_m, we found that they are located close to interesting radio sources and blazar candidates worthwhile of further investigations.

Other clusters, when analysed in a restricted field, dissolve into small non-significant structures, and therefore can be related to an increase of the local background instead of a genuine source. For example, in the case of the cluster 9Y-MST J0009−3249 of 12 photons and the very large $R_{max} = 37.'6$, at the Galactic latitude $b = -79.^\circ365$ and at the angular distance of $4.'7$ from a D^{3}PO structure (Selig et al. 2015), we found that it disappears by applying a Λ_{cut} value just below that used in the primary selection.

7. Roma-BZCAT blazars in the 9Y-MST catalogue

Blazars of the two main types, i.e. BL Lac objects and flat spectrum radio quasars (FSRQ), are the richest class of high-energy γ-ray sources. For this reason, it is interesting to investigate which clusters in the full 9Y-MST catalogue have a well-established association with the known and candidate blazars in the fifth edition of the Roma-BZCAT. This catalogue contains 3561 radio detected AGNs divided into three main types: BL Lac objects, candidates, and galaxy-dominated blazars (BZB and BZG, 1428 sources), FSRQ (BZQ, 1909 sources), plus a rather small sample of sources of uncertain type (BZU, 224 sources). The search for counterparts with all the entries in the catalogues gave 726 associations within $6'$ and 738 associations within $8'$, 7 of which are double associations and are discussed at the end of this section. The mean angular separaton is $\langle\delta\rangle = 1.'65$, that is much lower than the PSF radius at these energies, confirming the good estimates of the centroid coordinates given by our method. Only 12 sources were found with $6' < \delta < 8'$, but for 10 of these sources their R_{max} were from ∼25% to more than 3 times larger than δ; thus these associations cannot be excluded.

Two clusters (9Y-MST J2231−4422 and 9Y-MST J2358−4602) are located at δ values from the candidate counterparts comparable or larger than their R_{max}, thus the possibility that they were spurious association due to random closeness must be taken into account. Moreover, these two clusters have 3FGL sources at δ values of $5.'6$ and $10.'5$, respectively.

To verify the possibility of spurious associations we also searched for counterparts that have an angular distance to the cluster centroid higher than the corresponding R_{max}. In the sample of 738 associated blazars, only 3 did not satisfy this criterion: one is 9Y-MST J2358−4602, reported above, and the other two are 2 clusters of only 4 photons, very high clustering factors and R_{max} lower than $4'$. There is no statistical tool to establish if the associations of these two clusters were spurious or not, but considering that they were found to be positionally associated with FL8Y sources the most likely indication is for a genuine result.

The large majority of blazars related to γ-ray clusters are already in the 3FGL and 3FHL catalogues, while there are 34 associations with newly discovered 9Y-MST clusters with $\delta < 6'$, however 12 are already in the 1BIGB sample. Thus, our new detections of known blazars above 10 GeV are 22.

Finally, our results confirm that the richest class of high-energy γ-ray emitters are BL Lac objects with 548 sources, i.e. a percentage of about the 74% of the total sample, while FSRQs are 155 (∼21%) and 35 (∼4%) belong to those with uncertain classification. This finding is even more relevant in the subsample of Table A.1, in which there are 16 BL Lac objects that are counterpart candidates of which another 4 galaxy-dominated candidates must be added, while there are only 3 clusters with a possible association to FSRQ.

As reported above, we found that seven 9Y-MST clusters can be associated with a pair of fifth Roma-BZCAT sources within the angular distance of 8′. These rare cases can be due either to a single genuine association with a source in proximity of another blazar or to a real confusion if both sources are γ-ray loud.

To discriminate between these two possibilities we performed a new MST analysis in small regions surrounding these clusters to verify if they are fragmented into more components when lower $\Lambda_{\rm cut}$ values are used. For five of the seven clusters with a double blazar association, even performing a cluster search with $\Lambda_{\rm cut}$ values as low as $0.2\,\Lambda_m$, we always obtained single clusters with R_m and $R_{\rm max}$ smaller enough to exclude the more distant blazar as a counterpart. The source confusion only remains in the two cases of 9Y-MST J0009+0627 and 9Y-MST J0442−0019 because the possible counterparts are found to be very close to the cluster centroids even with the shortest $\Lambda_{\rm cut}$ values. More precisely, the former cluster with R_m = 3.′1 and $R_{\rm max}$ = 10.′2 has two blazars, 5BZQ J0009+0625 and 5BZB J0009+0628, at δ equal to 2.′1 and 2.′6, respectively, and the latter (R_m = 6.′1, $R_{\rm max}$ = 20.′6) has 5BZB J0323−0111 and 5BZB J0323−0108 at 1.′5 and 5.′6, respectively.

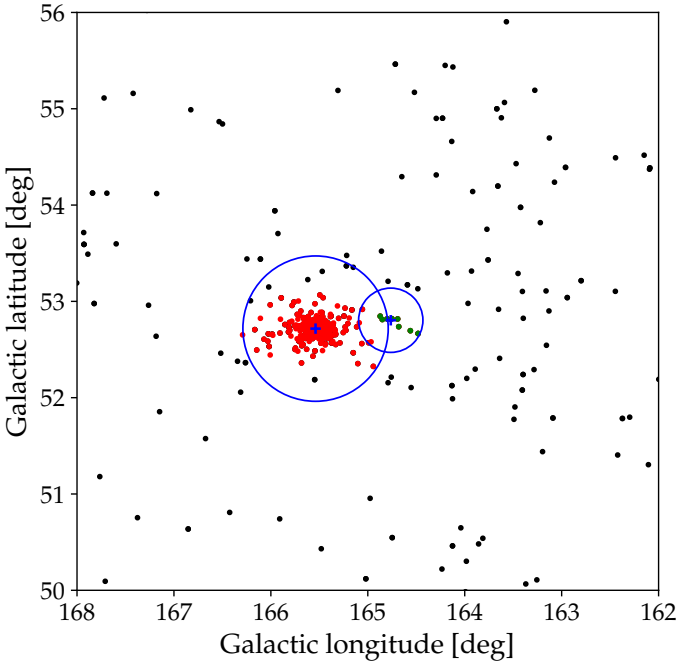

Fig. 10. Photon map at energies higher than 10 GeV in the sky region around the bright BL Lac object 1ES 1011+496. Photons in the rich cluster corresponding to the source are reported in red, while the green points are the 8 photons in the cluster 9Y-MST J1016+4949, likely a satellite of the former. Crosses indicate the centroid positions and the radii of the circles represent their $R_{\rm max}$.

8. High-energy unassociated clusters

As reported in Sect. 5, after having removed the clusters corresponding to the high-energy associations discussed in the preceding Sections, we obtained 249 clusters not corresponding to any source in the published *Fermi* catalogues or in the LMC (but including 89 new sources in the preliminary FL8Y list).

We also searched for positional correspondences between these clusters and objects in catalogues of possible blazars selected on the basis of the occurrence of some features typical of this class of active galactic nuclei (AGNs). The catalogues used were CRATES (Healey et al. 2007), which reports 11,131 flat spectrum radio sources; WIBRaLS (WISE Blazar-like Radio-loud Sources; D'Abrusco et al. 2014), which lists 7855 sources with mid-infrared colours typical of blazars; and 2WHSP (Chang et al. 2017), a multi-frequency catalogue of 1691 high-energy and very high-energy γ-ray blazars and blazar candidates. Considering that in all the three catalogues the source coordinates are known with a high accuracy, we considered angular distances lower than 6′ for possible associations with γ-ray clusters, which agrees with the angular distance distribution given in Fig. 7. The 22 BZCAT objects already found in the previous search were excluded to avoid redundant associations (Sect. 7).

The resulting associations were 15 clusters with CRATES sources, 14 with WIBRaLS, and 15 with 2WHSP, but some are common to two or to all three samples. The final number of clusters associated with entries of any of these three catalogues is 28 and they are indicated by a specific note in Table A.1.

The nature of the remaining unassociated clusters can be somewhat complex and several effects must be taken into account. As discussed in Sect. 3.3, there are several clusters that have values of R_m and $R_{\rm max}$ in excess with respect to those generally found for clusters associated with point-like sources. In Table A.1, large size clusters likely corresponding with extended structure are indicated by "ex". When investigated in rather small regions and with decreasing separation lengths, several clusters have an inner compact structure with radial values in agreement with those typical for clusters with a comparable photon number. We indicate these with the note "cc+ex". In the same analysis other clusters dissolve in non-significant structures and likely should be considered spurious, and for this reason they have the annotation "sp".

Another interesting possibility is the occurrence of possible satellite clusters, i.e. rather small clusters found at a relatively short distance from a much richer cluster. In principle, the nodes (i.e. the photon arrival directions) might belong to a unique cluster, but they were partitioned in two because of the occurrence of only one edge slightly longer than the separation distance. A satellite cluster usually has a g value and a photon number much lower that those of the nearby main cluster. Other possibilities are the occurrence of an extended emission, or of a single weak cluster embedded in a relatively high photon density region, and of a pair of close weak clusters.

We searched for satellites applying the simple criterion of sorting all cluster pairs having an angular separation of their centroids lower than the sum of their $R_{\rm max}$. Close weak clusters are expected to be resolved by a local MST analysis with a shorter $\Lambda_{\rm cut}$, while an extended emission would preferably fragment into a few low significance features.

The results of this search include two triplets, one of which (already mentioned above) in the region of the Large Magellanic Cloud. The second triplet is in the environment of the rich cluster 9Y-MST J1512−0906 (343 photons) associated with a 3FGL/3FHL source and with the bright FSRQ PKS 1510−089. The two other clusters are 9Y-MST J1508−0904, an unassociated low g cluster (thus a reliable satellite candidate), and the much more distant 9Y-MST J1514−0948, close to a 3FHL source and to one of the previously detected MST blazars (Paper III). We found 9 pairs of poor clusters close to much richer clusters, 8 of which are unassociated. An example is shown in Fig. 10, in which the photons in a rather small sky region around the BL Lac object 1ES 1011+496 and the two MST-found clusters are plotted: the richer cluster (370 photons)

is that associated with the blazar, while a much smaller unassociated cluster is found within the $R_{\rm max}$ distance.

The rich cluster 9Y-MST J2139−4235 with 107 photons and $R_{\rm max}$ = 39.′5 has the companion 9Y-MST J2138−4312 at 38.′2. The latter appears to be a significant structure (N = 8 and M = 30.08) instead of a satellite; moreover, it is at 4.′4 to a X-ray loud AGN with blazar mid-IR colours, enforcing this conclusion.

There are also 6 pairs with both clusters well associated with already known γ-ray sources. These cases must be considered as resolved with the $\Lambda_{\rm cut}$ employed. The 4 remaining pairs have unassociated clusters with a rather low number of photons: their classification as satellites is therefore uncertain because the occurrence of extended regions or of low significance close features cannot be excluded.

9. Summary and discussion

We analysed the first 9 years of *Fermi*-LAT data, using the Pass 8 events at energies higher than 10 GeV by means of the MST algorithm for detecting photon clusters. In the selection procedure we adopted severe threshold values to reduce the possibility of spurious detections due to local background fluctuations. We limited our search to the Galactic regions with $|b| > 20^\circ$ to avoid confusion problems in the Galactic belt due to its high photon density, which makes the choice of the best separation length difficult.

A new catalogue of 1342 clusters was obtained. The large majority of these clusters have a close spatial correspondence with γ-ray sources reported in the *Fermi* collaboration catalogues, but new γ-ray sources are detected through different multiwavelength searches and some others are found in the more recent preliminary FL8Y list. With respect to the 3FHL catalogue, which has 986 sources in the regions with a Galactic latitude higher than 20°, the number of 9Y-MST clusters is increased by about 36%. The sample of new detections contains 249 entries and is reported in Table A.1. Of these, 89 are also in the FL8Y list, thus there is a residual sample of 160 new γ-ray clusters. The search in catalogues of objects dominated by non-thermal emission in different electromagnetic bands gave 46 possible associations. We also searched for new possible blazar candidates within a region centred at the cluster centroid coordinates and having a radius of 6′. The search was based on possible optical or IR counterparts of radio sources, when present, or of quasars or candidates reported in large databases. Thus, 53 candidate objects were selected, whose blazar nature cannot be considered as confirmed since optical spectra are generally not available and in some cases there are no radio detections because their flux densities could be lower than the survey limits. A more detailed analysis of these objects will be presented in a forthcoming paper. Ultimately, there are 62 clusters without any confirmed or possible counterpart (of which 19 are classified as possible satellites or spurious clusters) i.e. less than 5% of the catalogue. This figure confirms the efficiency of the method and selection criteria.

As known from other high-energy catalogues, the large majority of clusters is associated with blazars and particularly with BL Lac objects (see Sect. 7). The continuous observation of the entire sky by *Fermi*-LAT over period of about a decade can enrich our knowledge of the population properties of this class of AGNs. It can be expected that the study of faint γ-ray sources can lead to the discovery of semi-quiescent or rarely flaring blazars, i.e. galactic nuclei exhibiting only occasionally bright high-energy bursts and remaining for rather long times in states too faint to allow their inclusion in sample based on a few "shot-like" measurements.

Acknowledgements. We acknowledge use of archival *Fermi* data. We made large use of the on-line version of the Roma-BZCAT and the scientific tools developed at the ASI Science Data Center (ASDC), the final release of 6dFGS archive, the Sloan Digital Sky Survey (SDSS) archive, the NED database, and other astronomical catalogues distributed in digital form (Vizier and Simbad) at Centre de Dates astronomiques de Strasbourg (CDS) at the Louis Pasteur University.

References

Abdo, A. A., Ackermann, M., Ajello, M., et al. 2010, ApJS, 188, 405
Acero, F., Ackermann, M., Ajello, M., et al. 2015, ApJS, 218, 23
Ackermann, M., Ajello, M., Albert, A., et al. 2012, ApJS, 203, 4
Ackermann, M., Ajello, M., Allafort, A., et al. 2013a, ApJ, 765, 54
Ackermann, M., Ajello, M., Allafort, A., et al. 2013b, ApJS, 209, 34
Ackermann, M., Ajello, M., Asano, K., et al. 2014, Science, 343, 42
Ajello, M., Atwood, W. B., Baldini, L., et al. 2017, ApJS, 232, 18
Armstrong, T., Brown, A. M., Chadwick, P. M., & Nolan, S. J. 2015, MNRAS, 452, 3159
Arsioli, B., & Chang, Y.-L. 2017, A&A, 598, A134
Arsioli, B., Fraga, B., Giommi, P., Padovani, P., & Marrese, P. M. 2015, A&A, 579, A34
Asvathaman, A., Omand, C., Barton, A., & Heyl, J. S. 2017, MNRAS, 466, 2378
Bignami, G. F., Boella, G., Burger, J. J., et al. 1975, Space Sci. Instrum., 1, 245
Buson, S. 2016, ATel, 9285
Campana, R., Massaro, E., Gasparrini, D., Cutini, S., & Tramacere, A. 2008, MNRAS, 383, 1166
Campana, R., Bernieri, E., Massaro, E., Tinebra, F., & Tosti, G. 2013, Ap&SS, 347, 169
Campana, R., Massaro, E., Bernieri, E., & D'Amato, Q. 2015, Ap&SS, 360, 19
Campana, R., Massaro, E., & Bernieri, E. 2016a, Ap&SS, 361, 367
Campana, R., Massaro, E., & Bernieri, E. 2016b, Ap&SS, 361, 185
Campana, R., Massaro, E., & Bernieri, E. 2016c, Ap&SS, 361, 183
Campana, R., Massaro, E., & Bernieri, E. 2018, Ap&SS, 363, 144
Chang, Y.-L., Arsioli, B., Giommi, P., & Padovani, P. 2017, A&A, 598, A17
Chornock, R., & Margutti, R. 2017, ATel, 10491
Ciprini, S., Tosti, G., Marcucci, F., et al. 2007, in The First GLAST Symposium, eds. S. Ritz, P. Michelson, & C. A. Meegan, AIP Conf. Ser., 921, 547
Ciprini, S., Cheung, C. C., Kocevski, D., et al. 2017, ATel, 10482
D'Abrusco, R., Massaro, F., Paggi, A., et al. 2014, ApJS, 215, 14
Damiani, F., Maggio, A., Micela, G., & Sciortino, S. 1997, ApJ, 483, 350
Di Gesù, V., & Sacco, B. 1983, Pattern Recognit., 16, 525
Healey, S. E., Romani, R. W., Taylor, G. B., et al. 2007, ApJS, 171, 61
Kawase, T., Negoro, H., Ueno, S. et al. 2017, ATel, 10495
Maselli, A., Melandri, A., Nava, L., et al. 2014, Science, 343, 48
Massaro, E., Maselli, A., Leto, C., et al. 2014, in Multifrequency Catalogue of Blazars, 5th ed. (Rome: Aracne Editrice)
Massaro, E., Maselli, A., Leto, C., et al. 2015, Ap&SS, 357, 75
Mattox, J. R., Bertsch, D. L., Chiang, J., et al. 1996, ApJ, 461, 396
Nolan, P. L., Abdo, A. A., Ackermann, M., et al. 2012, ApJS, 199, 31
Prim, R. 1957, Bell System Tech. J., 36, 1389
Selig, M., Vacca, V., Oppermann, N., & Enßlin, T. A. 2015, A&A, 581, A126
Su, M., Slatyer, T. R., & Finkbeiner, D. P. 2010, ApJ, 724, 1044
Tramacere, A., & Vecchio, C. 2013, A&A, 549, A138

Appendix A: Additional table

Table A.1. Sources in the 9Y-MST catalogue unassociated with any *Fermi*-LAT catalogue.

Name	RA (J2000) °	Dec (J2000) °	l °	b °	N	g	M	R_m ′	$R_{\max}$ ′	Notes
9Y-MST J0000−0216	0.104	−2.272	94.596	−62.303	4	4.398	17.594	2.8	5.9	BZc
9Y-MST J0009+0855	2.364	8.923	105.723	−52.540	5	5.909	29.544	1.6	4.1	
9Y-MST J0009−1418	2.379	−14.306	83.530	−73.878	4	3.540	14.160	3.1	7.2	FL8Y
9Y-MST J0009−3249	2.482	−32.828	358.036	−79.365	12	2.002	24.025	21.0	37.6	sp, ex
9Y-MST J0012−0429	3.037	−4.487	98.725	−65.495	9	2.057	18.516	10.7	18.4	sp, ex
9Y-MST J0012−1939	3.191	−19.655	71.020	−78.407	4	5.650	22.598	2.2	5.5	
9Y-MST J0013−3222	3.439	−32.373	357.984	−80.291	10	2.319	23.194	12.7	24.7	sp?, ex, BZc
9Y-MST J0015+0149	3.769	1.826	104.665	−59.750	4	4.481	17.924	1.8	4.0	
9Y-MST J0015+2441	3.989	24.686	112.762	−37.484	4	5.224	20.896	1.1	4.1	WB, FL8Y
9Y-MST J0019−0918	4.855	−9.306	98.441	−70.640	10	2.588	25.879	8.8	22.4	cc+ex
9Y-MST J0019+3626	4.926	36.449	115.837	−25.985	5	4.494	22.468	2.3	4.0	
9Y-MST J0021−5918	5.302	−59.314	310.087	−57.392	4	13.245	52.981	0.7	1.2	BZc, FL8Y
9Y-MST J0024+2401	6.028	24.027	114.961	−38.421	8	2.618	20.942	5.0	11.9	BZc, FL8Y
9Y-MST J0025−1911	6.439	−19.186	84.996	−80.109	8	2.296	18.370	11.2	25.4	sp, ex
9Y-MST J0030−5643	7.529	−56.724	308.812	−60.160	13	2.444	31.771	9.5	21.2	FL8Y
9Y-MST J0032−1908	8.128	−19.136	93.401	−80.903	10	2.370	23.705	8.5	19.9	
9Y-MST J0032−5541	8.132	−55.688	308.472	−61.236	6	3.222	19.331	3.7	12.4	
9Y-MST J0035−1740	8.830	−17.671	100.630	−79.837	4	4.928	19.712	2.0	5.0	FL8Y
9Y-MST J0035−2639	8.861	−26.666	39.412	−86.404	4	3.708	14.833	1.6	13.6	
9Y-MST J0043−1936	10.920	−19.602	109.228	−82.267	4	3.513	14.051	6.5	12.1	
9Y-MST J0045−2023	11.495	−20.385	112.157	−83.142	9	3.129	28.159	8.9	21.4	BZc, FL8Y
9Y-MST J0048−2427	12.138	−24.457	109.110	−87.251	6	4.892	29.351	2.9	11.7	WB, FL8Y
9Y-MST J0049+2252	12.278	22.871	122.233	−39.997	4	6.869	27.476	0.7	3.4	CR, FL8Y
9Y-MST J0056−3600	14.000	−36.013	296.983	−81.063	8	2.492	19.934	10.8	22.0	sp, ex
9Y-MST J0058−1433	14.562	−14.55	130.459	−77.322	4	4.599	18.398	0.9	8.0	2W
9Y-MST J0112−3159	18.170	−31.987	260.661	−83.298	4	3.673	14.690	3.2	8.9	5BZB
9Y-MST J0117−2444	19.352	−24.744	192.161	−83.694	5	3.560	17.801	4.4	15.1	5BZB, FL8Y
9Y-MST J0119−2739	19.884	−27.661	219.428	−83.741	7	3.170	22.191	8.0	15.8	ex, ps
9Y-MST J0119−0922	19.910	−9.369	144.810	−71.033	4	3.719	14.874	2.6	6.4	
9Y-MST J0121−7216	20.309	−72.27	299.749	−44.673	6	5.472	32.832	2.8	3.6	BZc
9Y-MST J0122−3004	20.539	−30.074	238.337	−82.644	5	6.795	33.974	1.9	4.6	BZc, FL8Y
9Y-MST J0122+1033	20.617	10.553	135.260	−51.575	4	3.815	15.262	1.1	8.1	BZc
9Y-MST J0124−3432	21.155	−34.542	261.142	−79.727	8	2.460	19.678	12.1	17.2	sp, ex
9Y-MST J0127+1737	21.984	17.627	135.140	−44.378	4	6.428	25.710	1.4	3.3	BZc
9Y-MST J0129+1229	22.393	12.484	137.296	−49.321	4	4.241	16.962	2.6	4.1	
9Y-MST J0133−4237	23.331	−42.617	276.802	−72.322	7	2.617	18.317	6.1	11.9	
9Y-MST J0142−0541	25.647	−5.696	154.809	−65.352	5	3.852	19.262	2.8	5.6	5BZB, CR, WB, FL8Y
9Y-MST J0143−0122	25.855	−1.373	150.930	−61.386	5	3.541	17.706	2.5	6.3	BZc

Notes. See main text for details. Column N gives the number of photons in the MST cluster, g its clustering degree and $M = Ng$ its magnitude. Meaning of the annotation is the following: FL8Y: cluster with a correspondent source in the FL8Y list within 6′; LMC: cluster in the Large Magellanic Cloud; BZc: possible blazar candidate; WB: possible counterpart in the WIBRaLS sample; CR: possible counterpart in the CRATES catalogue; 2W: possible counterpart in the 2WSHP catalogue; 5BZB: cluster with a correspondent BL Lac object in the 5BZCAT; 5BZQ: cluster with a correspondent FSRQ in the 5BZCAT; 5BZG: cluster with a correspondent galaxy-dominated blazar in the 5BZCAT; AGN: possible AGN counterpart; sp: possible spurious cluster due to background fluctuations; spp: very likely spurious cluster due to background fluctuations; ps: possible satellite cluster; ex: extended cluster; c+ex: extended cluster with interesting core structure; cc+ex: extended cluster with compact core; and ccc+ex: extended cluster with a significant compact core.

Table A.1. continued.

Name	RA (J2000) °	Dec (J2000) °	l °	b °	N	g	M	R_m ′	$R_{\max}$ ′	Notes
9Y-MST J0151−4037	27.845	−40.633	264.272	−71.692	9	2.613	23.514	8.3	22.9	ex, BZc
9Y-MST J0202−3531	30.584	−35.529	246.387	−72.725	5	5.467	27.337	2.6	4.1	
9Y-MST J0202+2942	30.637	29.709	140.890	−30.670	9	2.953	26.581	7.6	16.0	BZc, FL8Y
9Y-MST J0202−4042	30.680	−40.701	260.213	−70.001	4	4.404	17.615	2.6	4.4	
9Y-MST J0204−1410	31.038	−14.167	179.168	−68.662	4	3.740	14.959	3.0	5.9	
9Y-MST J0204−0159	31.051	−1.986	160.742	−59.406	6	4.600	27.597	1.9	9.7	
9Y-MST J0208−3116	32.187	−31.268	231.341	−72.653	4	4.320	17.281	3.4	4.8	BZc
9Y-MST J0215−1619	33.787	−16.319	188.094	−67.806	4	4.506	18.025	2.5	4.4	2W
9Y-MST J0225−1511	36.437	−15.198	189.164	−65.054	4	3.608	14.433	3.7	5.4	
9Y-MST J0226−5944	36.505	−59.737	283.026	−53.582	4	4.863	19.450	2.2	3.6	
9Y-MST J0232−1120	38.158	−11.339	184.250	−61.471	5	6.269	31.343	1.6	5.0	FL8Y
9Y-MST J0239−2019	39.973	−20.326	203.441	−64.322	8	2.256	18.047	7.2	20.1	sp, ex
9Y-MST J0240+1431	40.005	14.519	158.577	−40.719	4	4.970	19.878	2.4	2.7	WB
9Y-MST J0241−1602	40.458	−16.042	195.194	−62.131	7	4.005	28.033	3.7	7.0	2W, FL8Y
9Y-MST J0245−0251	41.361	−2.857	176.184	−53.502	4	6.303	25.214	1.4	2.5	WB, FL8Y
9Y-MST J0246−3349	41.674	−33.826	235.148	−64.374	5	3.976	19.879	2.9	6.2	BZc, FL8Y
9Y-MST J0247+2232	41.972	22.547	155.291	−32.907	8	2.537	20.295	6.2	12.1	FL8Y
9Y-MST J0259−1706	44.889	−17.101	200.930	−58.786	6	5.708	34.248	1.7	5.7	BZc, FL8Y
9Y-MST J0308−4702	47.248	−47.034	258.655	−56.537	5	4.258	21.290	1.1	7.4	FL8Y
9Y-MST J0315−4757	48.801	−47.964	259.409	−55.200	4	3.753	15.012	4.5	5.6	FL8Y
9Y-MST J0315−2643	48.850	−26.732	220.617	−58.022	5	3.827	19.137	1.6	8.8	FL8Y
9Y-MST J0324+3034	51.202	30.567	158.014	−21.663	11	2.794	30.737	10.3	14.1	BZc
9Y-MST J0328+3122	52.156	31.375	158.198	−20.526	15	3.032	45.483	7.8	14.5	AGN
9Y-MST J0332−7041	53.038	−70.691	286.529	−40.934	6	4.882	29.289	3.2	5.7	2W
9Y-MST J0332+8227	53.103	82.451	128.158	21.271	9	2.761	24.848	4.7	10.7	BZc, FL8Y
9Y-MST J0332+3102	53.234	31.045	159.193	−20.227	24	1.980	47.529	17.0	30.9	sp, ex, FL8Y
9Y-MST J0334−3839	53.743	−38.654	242.219	−54.123	6	3.024	18.141	3.7	8.7	
9Y-MST J0336+0302	54.247	3.041	182.436	−39.985	4	4.019	16.075	2.5	7.0	
9Y-MST J0357+1815	59.332	18.263	172.962	−26.051	6	4.150	24.902	1.9	6.8	
9Y-MST J0404−1713	61.024	−17.231	210.771	−44.592	7	2.967	20.769	5.1	11.5	BZc, FL8Y
9Y-MST J0416+1901	64.038	19.018	175.674	−22.265	4	4.776	19.106	1.4	3.5	
9Y-MST J0428+1846	67.129	18.777	177.911	−20.2	9	2.450	22.049	7.3	14.4	
9Y-MST J0430+1322	67.532	13.373	182.711	−23.28	8	2.811	22.484	3.6	16.1	cc+ex
9Y-MST J0455−5434	73.970	−54.580	262.597	−38.374	4	4.345	17.381	2.0	2.8	
9Y-MST J0525−6556	81.395	−65.936	275.927	−33.309	6	3.775	22.649	2.8	6.4	
9Y-MST J0526−0259	81.646	−2.996	205.692	−20.208	4	4.44	17.759	1.9	3.5	
9Y-MST J0526−1518	81.668	−15.311	217.765	−25.512	7	4.078	28.549	2.9	5.7	2W, FL8Y
9Y-MST J0529−6829	82.492	−68.491	278.871	−32.534	4	4.442	17.770	1.3	4.7	LMC
9Y-MST J0533−6926	83.466	−69.436	279.920	−32.055	12	2.444	29.324	8.2	16.7	LMC
9Y-MST J0557+7705	89.392	77.087	136.637	23.461	6	3.883	23.296	3.7	6.8	BZc, FL8Y
9Y-MST J0641−7904	100.457	−79.076	290.658	−27.052	4	4.412	17.649	1.2	5.1	
9Y-MST J0650−5146	102.563	−51.767	261.357	−21.163	11	3.471	38.178	3.5	11.8	BZc, FL8Y
9Y-MST J0709+4304	107.264	43.075	174.291	21.183	4	7.057	28.229	1.1	1.7	FL8Y

Table A.1. continued.

Name	RA (J2000) °	Dec (J2000) °	l °	b °	N	g	M	R_m ′	$R_{\max}$ ′	Notes
9Y-MST J0709+4838	107.304	48.635	168.559	22.818	7	4.311	30.176	2.8	9.3	CR, FL8Y
9Y-MST J0715−6829	108.772	−68.494	279.596	−22.994	5	4.656	23.280	4.0	4.4	CR, WB, FL8Y
9Y-MST J0741+3226	115.252	32.448	187.331	23.943	4	4.522	18.088	2.2	3.4	5BZB, FL8Y
9Y-MST J0749+2312	117.325	23.216	197.470	22.585	4	7.634	30.536	1.5	2.2	5BZG, FL8Y
9Y-MST J0751+3314	117.953	33.235	187.244	26.344	4	5.059	20.236	2.1	4.3	5BZQ, CR, FL8Y
9Y-MST J0752+7120	118.177	71.341	143.912	30.480	4	5.017	20.069	1.7	2.5	BZc
9Y-MST J0816+4909	124.103	49.161	170.088	33.769	10	3.718	37.183	3.7	8.3	5BZB, WB, FL8Y
9Y-MST J0829+5232	127.486	52.540	166.029	35.980	4	4.583	18.332	2.2	5.9	2W, FL8Y
9Y-MST J0843+5031	130.753	50.525	168.473	38.074	6	4.853	29.121	3.6	5.8	2W
9Y-MST J0933+0125	143.267	1.418	232.692	36.016	4	4.813	19.251	1.5	4.4	
9Y-MST J0947+1120	146.991	11.349	223.883	44.213	4	4.926	19.702	1.6	4.2	BZc
9Y-MST J0950+0616	147.565	6.278	230.342	42.236	4	4.963	19.851	1.4	3.9	5BZB, CR, WB, FL8Y
9Y-MST J1003−2139	150.894	−21.661	258.935	26.533	5	5.611	28.057	2.0	5.6	BZc, FL8Y
9Y-MST J1003+7048	150.907	70.816	139.699	40.403	6	3.930	23.581	2.9	6.5	
9Y-MST J1006−3015	151.609	−30.26	265.521	20.376	4	4.514	18.057	2.0	4.1	
9Y-MST J1016+4949	154.175	49.829	164.763	52.804	8	3.498	27.983	3.9	13.2	
9Y-MST J1018+2210	154.599	22.175	212.496	55.009	6	3.595	21.571	3.2	6.8	FL8Y
9Y-MST J1044+3030	161.142	30.513	198.365	62.097	4	6.126	24.502	1.6	3.2	
9Y-MST J1057+5512	164.357	55.204	151.402	55.162	5	4.611	23.055	1.6	3.2	2W, FL8Y
9Y-MST J1103−3211	165.837	−32.195	277.756	25.339	4	4.308	17.231	2.1	5.0	
9Y-MST J1105−0625	166.369	−6.431	261.671	47.770	8	2.674	21.389	4.7	13.6	FL8Y
9Y-MST J1111+4857	167.991	48.955	157.580	60.941	4	4.762	19.046	0.7	5.3	2W, FL8Y
9Y-MST J1114+5521	168.554	55.365	148.179	56.738	8	2.575	20.602	5.4	8.4	FL8Y
9Y-MST J1114+0637	168.569	6.625	250.132	59.136	7	2.648	18.536	5.0	8.8	FL8Y
9Y-MST J1116+2916	169.138	29.270	201.497	69.021	7	2.810	19.671	3.9	12.1	AGN
9Y-MST J1124+2047	171.027	20.799	225.840	69.104	7	2.672	18.706	5.2	8.9	5BZB, FL8Y
9Y-MST J1149−4030	177.368	−40.500	290.379	20.857	4	10.919	43.676	0.8	1.6	CR, WB, FL8Y
9Y-MST J1150+4209	177.548	42.166	158.725	70.449	4	4.317	17.267	1.1	4.6	ps
9Y-MST J1153+3821	178.450	38.364	166.365	73.512	7	3.867	27.069	2.8	5.1	5BZB, WB, FL8Y
9Y-MST J1158−1430	179.726	−14.508	284.310	46.456	12	2.194	26.331	7.5	17.5	cc+ex, FL8Y
9Y-MST J1202+3857	180.516	38.954	160.887	74.318	5	3.697	18.483	2.8	3.8	BZc, FL8Y
9Y-MST J1210+3243	182.533	32.731	178.377	79.450	7	3.085	21.596	4.0	10.7	
9Y-MST J1210−2531	182.726	−25.519	291.547	36.455	4	4.498	17.991	2.0	2.8	2W
9Y-MST J1211+3903	182.905	39.055	155.275	75.469	5	3.683	18.417	3.4	7.4	5BZB, FL8Y
9Y-MST J1216−3734	184.009	−37.577	295.214	24.764	7	3.210	22.473	4.0	7.7	CR, WB, FL8Y
9Y-MST J1216+0932	184.065	9.535	276.014	70.546	6	3.158	18.950	4.6	8.3	5BZG, CR , FL8Y
9Y-MST J1219+0444	184.998	4.746	283.029	66.395	7	2.845	19.913	4.7	8.6	5BZB
9Y-MST J1227+2127	186.779	21.463	257.274	82.078	8	2.312	18.495	6.9	9.3	AGN
9Y-MST J1229+0012	187.417	−0.204	291.210	62.171	4	3.627	14.508	1.5	7.0	
9Y-MST J1237+3018	189.266	30.308	166.822	85.524	7	2.623	18.363	5.2	10.4	5BZB
9Y-MST J1246−2616	191.591	−26.273	301.516	36.584	9	2.571	23.138	7.9	17.0	cc+ex
9Y-MST J1254−1043	193.511	−10.729	303.975	52.137	5	4.013	20.063	2.0	6.4	
9Y-MST J1256−0606	194.016	−6.105	305.029	56.748	8	2.650	21.203	8.0	18.9	sp, ex, ps

Table A.1. continued.

Name	RA (J2000) °	Dec (J2000) °	l °	b °	N	g	M	R_m ′	$R_{\max}$ ′	Notes
9Y-MST J1256+0512	194.206	5.208	306.519	68.042	4	3.634	14.538	2.8	5.2	
9Y-MST J1257+2413	194.438	24.229	329.411	86.771	4	5.527	22.107	1.1	3.5	5BZB, FL8Y
9Y-MST J1258−0454	194.659	−4.901	306.310	57.923	7	3.225	22.574	5.1	10.1	FL8Y
9Y-MST J1306−1203	196.517	−12.060	308.578	50.651	4	4.338	17.351	2.1	4.1	
9Y-MST J1314−0900	198.720	−9.010	312.674	53.417	7	3.136	21.953	3.8	7.3	2W
9Y-MST J1318−1151	199.618	−11.854	313.357	50.470	9	2.403	21.628	7.7	19.4	cc, ex
9Y-MST J1326−0504	201.688	−5.073	319.094	56.687	6	5.009	30.057	2.4	6.1	5BZQ, CR, FL8Y
9Y-MST J1331−4158	202.856	−41.969	310.841	20.287	5	5.213	26.065	1.6	5.7	
9Y-MST J1332−0421	203.051	−4.357	321.839	57.011	4	3.839	15.354	1.9	6.2	
9Y-MST J1338−4200	204.545	−42.004	312.150	20.029	13	2.703	35.135	7.3	17.0	cc+ex, FL8Y
9Y-MST J1343+3558	205.915	35.979	74.7240	75.808	6	3.457	20.740	2.2	8.6	BZc
9Y-MST J1344+0718	206.244	7.315	338.035	66.466	10	2.120	21.202	10.9	21.5	cc+ex
9Y-MST J1345+1253	206.453	12.886	347.381	70.902	4	4.384	17.535	2.5	3.4	
9Y-MST J1352−1345	208.246	−13.760	324.905	46.469	4	4.196	16.785	1.7	5.5	
9Y-MST J1354+0153	208.509	1.892	336.296	60.643	5	4.368	21.839	2.3	3.5	5BZQ, CR, FL8Y
9Y-MST J1356−0107	209.123	−1.124	334.534	57.700	4	3.808	15.233	2.9	5.9	
9Y-MST J1359−1152	209.788	−11.874	327.969	47.679	6	3.366	20.198	3.2	11.8	FL8Y
9Y-MST J1359+1015	209.983	10.264	349.926	66.660	5	3.794	18.971	2.9	8.4	
9Y-MST J1400−4010	210.036	−40.169	316.904	20.831	9	3.963	35.665	2.8	12.2	2W, FL8Y
9Y-MST J1403+2432	210.928	24.539	27.923	73.547	6	3.304	19.822	3.8	8.0	
9Y-MST J1407−2708	211.837	−27.143	323.057	32.745	7	3.527	24.691	3.2	11.2	CR
9Y-MST J1409−1455	212.355	−14.929	329.509	43.882	9	2.258	20.318	7.4	12.3	
9Y-MST J1410+6057	212.621	60.959	106.862	53.634	5	4.299	21.496	3.2	4.7	5BZB
9Y-MST J1417+0432	214.498	4.550	349.180	59.411	4	6.480	25.919	0.8	3.8	BZc
9Y-MST J1420−2452	215.023	−24.882	327.243	33.770	8	2.504	20.033	6.0	11.8	
9Y-MST J1420−1438	215.173	−14.638	333.057	42.952	10	2.638	26.385	7.3	24.6	cc+ex
9Y-MST J1426+2415	216.703	24.252	30.649	68.355	6	4.444	26.666	1.6	7.0	5BZB
9Y-MST J1427+2321	216.964	23.357	28.469	67.909	8	2.515	20.120	4.1	8.6	
9Y-MST J1428−1443	217.133	−14.722	335.262	41.974	7	3.164	22.149	4.0	8.2	
9Y-MST J1428−1017	217.184	−10.287	338.453	45.768	8	3.147	25.179	4.3	11.8	
9Y-MST J1435−1109	218.877	−11.162	339.777	44.138	4	5.851	23.402	1.8	2.5	BZc
9Y-MST J1437+0542	219.483	5.711	357.517	56.830	4	4.304	17.215	2.0	5.2	
9Y-MST J1441+1830	220.389	18.508	19.965	63.271	8	2.723	21.786	4.4	11.9	WB, FL8Y
9Y-MST J1441−0454	220.443	−4.915	346.861	48.319	5	4.722	23.610	1.9	6.7	
9Y-MST J1455−0617	223.905	−6.296	349.463	45.064	11	2.931	32.243	6.7	16.4	cc+ex, BZc
9Y-MST J1458+4831	224.665	48.527	82.538	57.412	4	5.028	20.114	1.9	3.5	5BZB
9Y-MST J1508−0904	227.129	−9.074	350.267	40.871	9	2.579	23.211	7.8	15.4	sp, ex
9Y-MST J1517+0049	229.343	0.819	2.170	46.222	4	5.081	20.325	1.6	6.2	
9Y-MST J1520−0905	230.005	−9.091	352.977	38.937	7	3.143	22.000	3.5	9.7	WB, FL8Y
9Y-MST J1520−0525	230.020	−5.418	356.381	41.533	4	5.589	22.357	1.9	2.3	BZc
9Y-MST J1524−0818	231.105	−8.301	354.685	38.742	5	4.749	23.747	1.8	4.1	
9Y-MST J1525−1258	231.415	−12.970	350.914	35.162	9	2.513	22.617	8.9	17.1	sp, ex, BZc
9Y-MST J1528+2003	232.123	20.062	30.396	53.483	6	3.109	18.653	2.6	11.3	FL8Y

Table A.1. continued.

Name	RA (J2000) °	Dec (J2000) °	l °	b °	N	g	M	R_m ′	$R_{\max}$ ′	Notes
9Y-MST J1536−1147	234.148	−11.794	354.242	34.154	4	4.020	16.079	2.1	4.4	
9Y-MST J1537−1347	234.441	−13.796	352.794	32.533	14	2.166	30.317	6.9	16.6	cc+ex, FL8Y
9Y-MST J1552+1523	238.088	15.396	26.816	46.500	8	2.553	20.423	4.8	10.3	
9Y-MST J1556−0145	239.238	−1.763	7.646	36.847	8	2.901	23.209	4.8	14.1	BZc
9Y-MST J1604+0107	241.058	1.121	11.907	37.015	10	2.547	25.467	5.5	15.8	sp, ex
9Y-MST J1623+0449	245.887	4.826	18.938	34.871	5	4.289	21.445	2.9	5.3	
9Y-MST J1628+5347	247.179	53.794	82.394	42.420	4	4.065	16.259	1.4	4.8	
9Y-MST J1631+4143	247.949	41.732	65.948	43.128	6	3.569	21.414	2.2	6.3	BZc, FL8Y
9Y-MST J1632+0855	248.068	8.933	24.599	34.922	6	3.516	21.096	2.8	6.5	BZc, FL8Y
9Y-MST J1636−0456	249.104	−4.939	11.267	26.964	7	4.479	31.351	2.9	3.9	BZc
9Y-MST J1645−0745	251.269	−7.764	10.010	23.599	10	2.541	25.407	4.9	15.2	cc+ex, CR
9Y-MST J1646−0942	251.500	−9.708	8.409	22.311	10	3.583	35.831	3.5	7.6	BZc, FL8Y
9Y-MST J1647+2910	251.863	29.183	49.941	38.498	9	3.535	31.815	3.0	10.1	5BZG
9Y-MST J1652−1016	253.231	−10.267	8.954	20.589	12	2.121	25.446	7.8	12.0	
9Y-MST J1714+3227	258.647	32.450	55.491	33.551	9	5.249	47.241	2.4	5.8	BZc
9Y-MST J1724+3310	261.036	33.167	56.871	31.763	8	2.804	22.435	5.8	10.6	FL8Y
9Y-MST J1732+4445	263.095	44.752	70.662	32.327	5	4.689	23.444	1.0	7.8	
9Y-MST J1744+4636	266.048	46.603	73.146	30.542	4	4.560	18.239	1.8	3.5	BZc
9Y-MST J1759+5412	269.880	54.212	82.213	29.130	4	4.217	16.867	2.3	2.5	
9Y-MST J1759+7036	269.959	70.612	101.051	29.742	6	4.352	26.114	3.4	4.0	5BZB, FL8Y
9Y-MST J1815+3131	273.856	31.525	58.595	20.925	5	4.573	22.865	2.9	3.6	FL8Y
9Y-MST J1818−7122	274.739	−71.382	323.026	−23.078	10	2.347	23.469	6.7	20.3	cc+ex
9Y-MST J1845+7240	281.496	72.675	103.553	26.206	7	3.773	26.413	3.2	5.1	CR, FL8Y
9Y-MST J1947−3225	296.972	−32.418	7.846	−25.317	8	3.013	24.101	4.0	8.5	
9Y-MST J2018−0341	304.616	−3.696	39.779	−21.014	9	2.470	22.226	7.9	22.0	sp, ex
9Y-MST J2024−2234	306.219	−22.567	21.294	−30.056	12	2.785	33.424	4.7	13.1	BZc, FL8Y
9Y-MST J2025−3929	306.488	−39.499	1.914	−34.422	11	2.202	24.221	8.5	20.3	sp, ex, BZc
9Y-MST J2030−1622	307.714	−16.377	28.528	−29.174	9	3.014	27.127	2.8	9.2	BZc, FL8Y
9Y-MST J2034−3458	308.735	−34.980	7.715	−35.426	16	2.014	32.219	11.4	17.9	sp, ex
9Y-MST J2036−3042	309.123	−30.710	12.906	−34.852	4	4.773	19.090	1.6	2.8	
9Y-MST J2037−0501	309.491	−5.033	40.956	−25.939	10	2.333	23.329	7.4	16.1	BZc, FL8Y
9Y-MST J2038−3329	309.635	−33.496	9.682	−35.873	11	2.097	23.070	8.6	18.7	ex, ps, FL8Y
9Y-MST J2038−3654	309.662	−36.903	5.532	−36.492	7	3.139	21.971	3.3	9.9	
9Y-MST J2040−3915	310.231	−39.250	2.701	−37.256	4	4.415	17.661	2.8	4.0	
9Y-MST J2041−2848	310.467	−28.812	15.502	−35.530	4	4.268	17.072	1.8	4.0	
9Y-MST J2042−5323	310.560	−53.389	344.857	−37.789	8	2.918	23.340	3.9	13.3	
9Y-MST J2044−5611	311.100	−56.199	341.279	−37.820	12	2.141	25.695	9.1	17.9	sp, ex
9Y-MST J2044−3335	311.143	−33.596	9.857	−37.126	10	2.306	23.059	7.3	13.4	
9Y-MST J2046−5410	311.686	−54.175	343.786	−38.381	9	4.166	37.496	2.2	8.6	BZc, FL8Y
9Y-MST J2058−4307	314.510	−43.120	358.018	−40.735	4	4.094	16.378	2.3	4.8	
9Y-MST J2058−3339	314.537	−33.655	10.399	−39.921	4	5.415	21.661	1.3	2.9	BZc
9Y-MST J2101+0911	315.426	9.190	57.734	−23.583	9	2.503	22.529	6.4	14.8	2W, FL8Y
9Y-MST J2110+0740	317.622	7.673	57.748	−26.233	4	5.402	21.610	1.9	2.7	

Table A.1. continued.

Name	RA (J2000) $^\circ$	Dec (J2000) $^\circ$	l $^\circ$	b $^\circ$	N	g	M	R_m ′	$R_{\max}$ ′	Notes
9Y-MST J2114−3324	318.725	−33.415	11.384	−43.342	6	4.509	27.052	3.4	6.9	FL8Y
9Y-MST J2115−1546	318.839	−15.773	34.100	−38.838	8	2.607	20.857	5.8	14.0	
9Y-MST J2115−4938	318.916	−49.639	349.002	−43.368	5	7.052	35.259	1.9	2.9	BZc
9Y-MST J2120−0142	320.039	−1.710	50.286	−33.449	9	2.467	22.202	6.1	10.1	AGN
9Y-MST J2121−3131	320.382	−31.521	14.255	−44.466	5	4.307	21.537	2.4	3.7	
9Y-MST J2127−3840	321.761	−39.681	27.820	−46.161	8	2.716	21.730	5.9	11.2	
9Y-MST J2127−1533	321.969	−15.553	35.878	−41.537	4	4.823	19.292	1.6	5.7	
9Y-MST J2129−0933	322.464	−9.562	43.285	−39.436	4	4.832	19.328	1.1	4.7	
9Y-MST J2130−1310	322.584	−13.170	39.103	−41.126	9	2.327	20.943	6.2	13.9	
9Y-MST J2135−5759	323.829	−57.999	336.794	−44.101	6	4.057	24.341	2.6	8.6	BZc
9Y-MST J2136−3752	324.086	−37.869	5.430	−47.981	15	2.313	34.702	9.5	21.7	cc+ex
9Y-MST J2138−4312	324.663	−43.204	357.421	−48.124	8	3.760	30.076	4.9	11.1	BZc
9Y-MST J2140−4957	325.000	−49.953	347.494	−47.161	6	3.941	23.646	3.5	4.6	
9Y-MST J2144−8112	326.002	−81.212	310.564	−32.930	4	4.004	16.017	1.7	5.4	
9Y-MST J2147−3856	326.850	−38.936	3.716	−50.119	4	3.669	14.675	2.4	6.4	
9Y-MST J2151−4122	327.774	−41.367	359.824	−50.619	4	4.162	16.650	2.6	5.0	
9Y-MST J2151−3223	327.982	−32.398	14.027	−50.970	5	4.164	20.819	3.2	5.5	
9Y-MST J2159−3200	329.857	−32.002	14.849	−52.524	4	5.761	23.045	1.5	3.5	
9Y-MST J2201−3823	330.365	−38.399	4.276	−52.893	10	1.807	18.072	11.3	14.5	
9Y-MST J2232−2422	338.002	−24.368	30.033	−58.582	4	4.374	17.498	2.0	4.2	
9Y-MST J2234−4156	338.581	−41.939	356.033	−58.407	6	3.141	18.848	3.4	13.1	FL8Y
9Y-MST J2234−4018	338.679	−40.314	359.003	−58.917	4	3.510	14.040	3.9	6.1	
9Y-MST J2238−4909	339.744	−49.163	343.075	−56.349	9	2.065	18.585	11.5	26.0	sp, ex
9Y-MST J2240−1244	340.122	−12.738	51.567	−56.175	7	3.061	21.428	4.9	9.0	cc+ex, BZc, FL8Y
9Y-MST J2240−4747	340.185	−47.785	345.047	−57.254	8	3.858	30.863	1.8	17.3	BZc, FL8Y
9Y-MST J2241−4123	340.268	−41.384	356.334	−59.775	7	3.837	26.859	2.8	9.0	
9Y-MST J2241+2944	340.324	29.738	91.869	−25.170	10	3.336	33.357	3.8	10.8	FL8Y
9Y-MST J2310−4344	347.617	−43.740	347.086	−63.749	4	4.777	19.109	1.3	5.9	5BZG
9Y-MST J2319−0457	349.942	−4.958	74.289	−58.880	8	2.271	18.170	6.7	15.5	FL8Y
9Y-MST J2320+0704	350.128	7.073	86.888	−49.328	9	2.389	21.503	6.9	13.4	FL8Y
9Y-MST J2321−2606	350.445	−26.105	30.745	−69.962	5	4.954	24.769	2.8	6.0	BZc
9Y-MST J2323+2047	350.798	20.799	96.652	−37.529	4	6.534	26.135	1.5	2.6	FL8Y
9Y-MST J2325−2010	351.271	−20.176	47.697	−69.074	7	4.953	34.670	2.7	8.2	BZc, FL8Y
9Y-MST J2326−0200	351.700	−2.005	80.443	−57.718	7	2.642	18.491	6.6	12.5	BZc, FL8Y
9Y-MST J2328−1332	352.060	−13.546	63.751	−66.297	5	3.528	17.641	7.0	14.0	
9Y-MST J2331−3840	352.827	−38.668	353.29	−69.676	6	3.507	21.042	3.8	9.1	
9Y-MST J2331+0150	352.986	1.843	86.316	−55.274	7	2.792	19.543	5.1	8.6	
9Y-MST J2353+2809	358.421	28.166	107.738	−32.996	6	3.729	22.377	4.5	7.1	BZc
9Y-MST J2357−4835	359.278	−48.599	325.457	−66.085	10	2.393	23.935	9.5	17.0	cc+ex, CR, WB, FL8Y